Article

Cell

Per-Nucleus Crossover Covariation and Implications for Evolution

Graphical Abstract

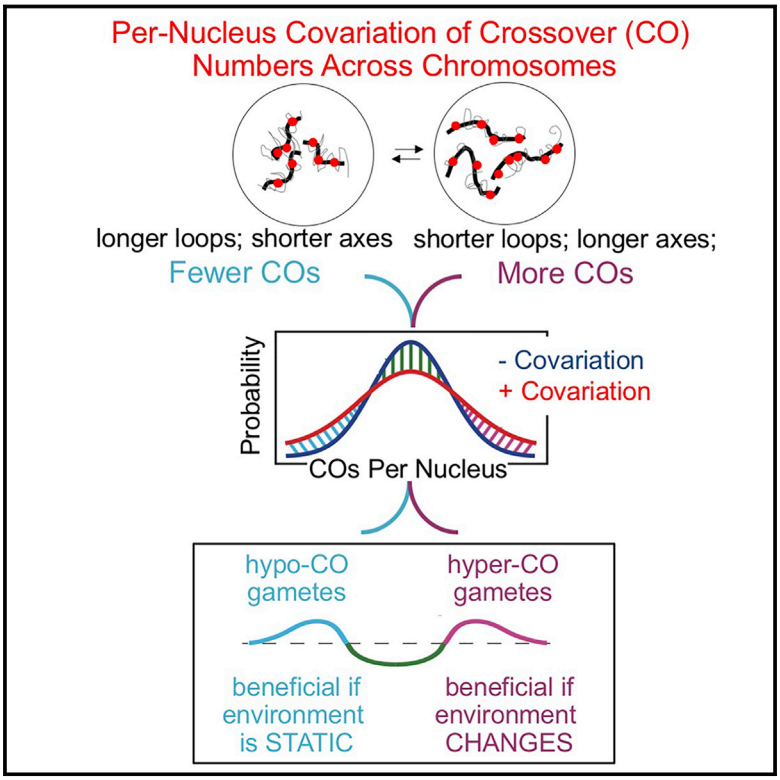

Highlights

- Crossover number is correlated across chromosomes within individual meiotic nuclei
- CO covariation results from covariation of chromosome axis lengths within nuclei
- CO covariation increases the frequencies of gametes with either many or few COs
- Hyper- and hypo-CO gametes aid adaptation in a sporadically fluctuating environment

Authors

Shunxin Wang, Carl Veller, Fei Sun, ..., Zijiang Chen, Nancy Kleckner, Liangran Zhang

Correspondence

kleckner@fas.harvard.edu (N.K.), shunxinwang@sdu.edu.cn (S.W.), zhangliangran@sdu.edu.cn (L.Z.)

In Brief

Crossover formation covaries within gametes generated by meiosis, leading to gametes with either many or few total crossovers, potentially representing a meiotic bet-hedging strategy to balance the evolutionarily advantages of recombination with its inherent risk.

Wang et al., 2019, Cell *177*, 326–338
April 4, 2019
https://doi.org/10.1016/j.cell.2019.02.021

CellPress

Cell

Article

Per-Nucleus Crossover Covariation and Implications for Evolution

Shunxin Wang,[1,11,*] Carl Veller,[2,3,11] Fei Sun,[4] Aurora Ruiz-Herrera,[5,6] Yongliang Shang,[1] Hongbin Liu,[1] Denise Zickler,[7] Zijiang Chen,[1] Nancy Kleckner,[8,12,*] and Liangran Zhang[1,9,10,*]

[1]Center for Reproductive Medicine, Shandong University, National Research Center for Assisted Reproductive Technology and Reproductive Genetics, Key Laboratory of Reproductive Endocrinology of Ministry of Education, Jinan, Shandong 250001, China
[2]Department of Organismic and Evolutionary Biology, Harvard University, Cambridge, MA 02138, USA
[3]Program for Evolutionary Dynamics, Harvard University, Cambridge, MA 02138, USA
[4]School of Medicine, Institute of Reproductive Medicine, Nantong University, Nantong, Jiangsu, China
[5]Genome Integrity and Instability Group, Institut de Biotecnologia i Biomedicina (IBB), Universitat Autònoma de Barcelona (UAB), Barcelona, Spain
[6]Departament de Biologia Cellular, Fisiologia i Immunologia, Universitat Autònoma de Barcelona (UAB), Barcelona, Spain
[7]Institute for Integrative Biology of the Cell (I2BC), CEA, CNRS, Université Paris-Sud, Université Paris-Saclay, Gif-sur-Yvette Cedex 91198, France
[8]Department of Molecular and Cellular Biology, Harvard University, Cambridge, MA 02138, USA
[9]Advanced Medical Research Institute, Shandong University, Jinan, Shandong 250014, China
[10]State Key Laboratory of Microbial Technology, Shandong University, Qingdao 266237, China
[11]These authors contributed equally
[12]Lead Contact
*Correspondence: shunxinwang@sdu.edu.cn (S.W.), kleckner@fas.harvard.edu (N.K.), zhangliangran@sdu.edu.cn (L.Z.)
https://doi.org/10.1016/j.cell.2019.02.021

SUMMARY

Crossing over is a nearly universal feature of sexual reproduction. Here, analysis of crossover numbers on a per-chromosome and per-nucleus basis reveals a fundamental, evolutionarily conserved feature of meiosis: within individual nuclei, crossover frequencies covary across different chromosomes. This effect results from per-nucleus covariation of chromosome axis lengths. Crossovers can promote evolutionary adaptation. However, the benefit of creating favorable new allelic combinations must outweigh the cost of disrupting existing favorable combinations. Covariation concomitantly increases the frequencies of gametes with especially high, or especially low, numbers of crossovers, and thus might concomitantly enhance the benefits of crossing over while reducing its costs. A four-locus population genetic model suggests that such an effect can pertain in situations where the environment fluctuates: hyper-crossover gametes are advantageous when the environment changes while hypo-crossover gametes are advantageous in periods of environmental stasis. These findings reveal a new feature of the basic meiotic program and suggest a possible adaptive advantage.

INTRODUCTION

Meiosis is the specialized cellular program that yields gametes for sexual reproduction. DNA recombination is a central feature of this program. Crossover (CO) recombination shuffles the alleles along chromosomes, leading to genetic diversity of gametes and thus progeny (Bell, 1982; Veller et al., 2019). The nearly universal occurrence of CO recombination in sexually reproducing organisms is assumed to imply a fundamental adaptive role (Maynard Smith, 1978). However, the ability of COs to create favorable new allelic combinations must be balanced against their seemingly opposing ability to break apart existing combinations that have been selected for. These opposing potentials are sometimes referred to as the "good" and "bad" effects of crossing over (Stapley et al., 2017; Otto, 2009).

In some organisms, this dilemma is addressed by alternation between sexual and asexual reproductive lifestyles, usually with the sexual phase involving dispersal to new environments and/or being triggered by information that the environment is changing (Williams, 1975; Bell, 1982). Other organisms utilize programmed variations of sexual reproduction in which recombination frequency is specifically elevated in conditions of stress, where new genetic combinations may be beneficial (Bell, 1982).

In the general case, including obligately sexual organisms, theoretical modeling suggests that the advantage of crossing over comes into play in at least two ways (Sharp and Otto, 2016). First, in the long-term evolution of populations, COs can accelerate adaptation by bringing together favorable alleles that would otherwise compete with one another and by separating favorable alleles from linked unfavorable alleles that otherwise would impede the spread of the favorable alleles (Hill and Robertson, 1966; Felsenstein, 1974; McDonald et al., 2016). Second, in conditions where the environment fluctuates in time or space, COs can generate previously rare (or absent) genetic combinations that allow immediate adaptation (Williams, 1975; Charlesworth, 1976; Maynard Smith, 1978; Sasaki and Iwasa, 1987; Hamilton et al., 1990).

Previous studies of crossing over, beginning with classic genetic analyses, primarily analyzed recombination patterns on a per-chromosome basis. Such studies revealed not only the occurrence of crossing over but also the phenomenon of CO interference, a one-dimensional spatial patterning process that results, ultimately, in even spacing of COs along each chromosome (Jones and Franklin, 2006). Here, we analyze CO patterns from a different perspective: with respect to the numbers of COs along individual chromosomes in single meiotic nuclei. Such information is provided by both cytological and DNA sequencing approaches.

Analysis of such data reveals a new basic feature of the meiotic recombination program: the numbers of CO-fated recombination interactions (and thus COs) tend to covary across different chromosomes, at higher or lower levels, within individual meiotic nuclei. Further, in accord with diverse evidences that axis length determines recombination and CO levels (Wang et al., 2017; see below), the proximate basis for this effect is analogous per-nucleus covariation of different chromosome axis lengths. Since chromosome axis length is known to be determined by chromatin loop length (e.g., Wang et al., 2017; see below), global loop-length modulation could underlie global modulation of CO frequencies.

Per-nucleus CO covariation results in an overdispersed distribution of total CO levels per nucleus. The practical consequence of this effect is to elevate the frequencies of nuclei, and thereafter gametes, that contain either very many or very few COs, coordinately on all chromosomes. This outcome triggered the idea that CO covariation might increase the ability of COs to promote evolutionary adaptation. Both hyper- and hypo-CO gametes would be available, at all times, to provide either more or less genetic shuffling according to the dictates of the circumstances. Using a four-locus population genetic model, we provide support for this adaptive advantage of CO covariation across a range of situations in which the environment fluctuates: hyper-CO gametes are advantageous when the environment changes while hypo-CO gametes are advantageous in periods of environmental stasis. These findings suggest that CO covariation, an intrinsic feature of the basic meiotic chromosomal program and apparently common to most sexual organisms, has the potential to increase the power of crossing over to enhance evolutionary adaptation.

Per-Nucleus Analysis of COs

Two methodologies can define the numbers and positions of CO events along each chromosome (bivalent) in individual meiotic nuclei: (1) cytological analysis and (2) DNA sequencing. (1) At the pachytene stage of meiotic prophase, the axes of homologous chromosomes are linked at ~100 nm along their lengths by a "pairing structure," the synaptonemal complex (SC). In spread chromosomal preparations subjected to immunofluorescent staining, the positions of all CO events, along each individual SC, are specifically marked by foci of particular proteins, e.g., MLH1 or Hei10-T3, as defined for many different organisms (e.g., Figures 1, S1C, and S1D). Cytological analyses can analogously define the numbers of foci that mark the sites of early recombination intermediates (e.g., replication protein A [RPA] or Hei10-T2; Figures S1A and S1B) as well as underlying SC lengths in the same nuclei at both the CO and early intermediate stages. (2) DNA sequence analysis has been applied only to a few organisms thus far. Data suitable for per-nucleus analysis are available from human female, where numbers and positions of COs along all chromosomes in individual nuclei are known for the egg and the two polar bodies of individual oocytes (Hou et al., 2013; Ottolini et al., 2015) and from individual human male sperm (Lu et al., 2012; Wang et al., 2012), which can be related to per-nucleus data (see below).

CO-associated cytologically defined foci accurately report final CO numbers. Where tested, their average number corresponds well to the average number of COs, detected either by DNA sequence analysis or as the number of chiasmata (the cytological manifestations of COs seen at diplotene). For example, analyses of human male report average numbers of 49.1 MLH1 foci (Gruhn et al., 2013; Wang et al., 2017), 49.6 chiasmata (Laurie and Hultén, 1985), 50.7 COs (sperm sequencing, Lu et al., 2012), and ~50 COs (pedigree studies such as HapMap, deCODE etc.; further discussions in Marcon and Moens, 2003; De Muyt et al., 2014; Anderson et al., 2014). This agreement reflects the fact that the period when CO foci are present is long lived and the number of foci remains stable throughout different substages (e.g., Marcon and Moens, 2003; De Muyt et al., 2014). Correspondingly, our analyses of DNA sequence data and CO focus data yield the same results (see below).

The Distribution of Total COs per Nucleus Is Overdispersed Relative to the Hypothesis of Independence across Chromosomes

Previous analyses by several methods show that the total number of CO events per nucleus varies significantly from one nucleus to another (e.g., Wang et al., 2017; Lynn et al., 2004; Sun et al., 2006; Ruiz-Herrera et al., 2017; Lu et al., 2012; Hou et al., 2013) (Figure 1A, left versus right; Table S1; see below). Such variability could simply reflect intrinsic variability in the numbers of COs on different chromosomes as determined independently on those different chromosomes (hereafter "intrinsic variation"). To investigate this possibility, we asked whether the experimental distribution of COs per nucleus corresponded to that predicted if all variation resulted from independent variability on different chromosomes. To do so, we pooled all of the bivalents analyzed in experimental data, separately for each chromosome, and then created artificial nuclei "in silico," each containing one bivalent of each chromosome drawn at random from the corresponding pool (STAR Methods). Analysis of human male data shows that the per-nucleus CO numbers observed experimentally vary much more widely than predicted from the artificial nuclei assembled *in silico* by the "hypothesis of independence," with coefficients of variation (CVs) of 0.1 and 0.05, respectively (Figures 1B and 1C, top, blue versus red; Figure S1E). As a result, the observed percentages of nuclei that contain either more or fewer COs are both substantially greater than those predicted by the hypothesis of independence for *in silico* nuclei (Figure 1C, top, blue versus red; bottom, blue and orange). For human male, hyper- and hypo-CO nuclei each comprise ~16% of the total. We define the sum of these percentages, ~32% in human male, as the "variability index" (VI) (Figure 1D, data and corresponding best-fit normal distributions "dist"; Figure S1F). The VI provides a useful quantitative

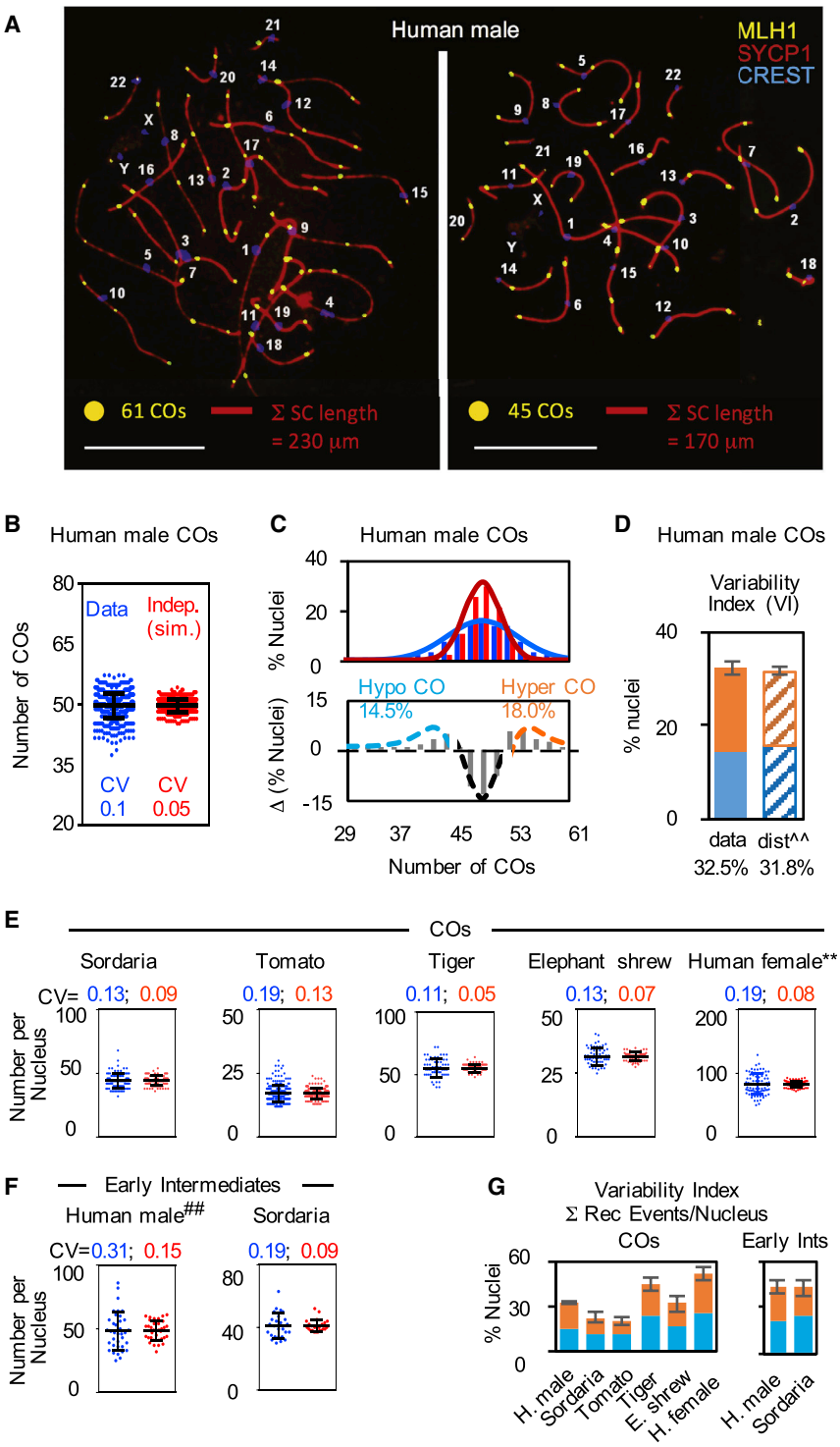

Figure 1. Per-Nucleus Analysis of COs

(A) Human male pachytene nuclei immunostained for synaptonemal complex (SYCP1; red), CO recombination complexes (MLH1; yellow) and centromeres (CREST; blue) for 22 autosomes. Nuclei with longer axes and more COs (left) or shorter axes and fewer COs (right) are illustrated. Images provided by F. Sun. Scale bars, 10 µm. See also Figures S1A–S1D.

(B–G) Overdispersed distribution of total COs per nucleus and resultant hyper- and hypo-CO nuclei. (B and C, top). Experimental distribution of total CO number per nucleus in human male pachytene nuclei (blue; n = 755) is compared with the distribution predicted if COs were determined independently on different chromosomes (the hypothesis of independence for *in silico* nuclei; text; red). Solid lines are best-fit normal distributions (C top; details in Figure S2A). The difference between these two distributions defines the frequencies of hypo- and hyper-CO nuclei (C bottom; blue, orange).

(D) The sum of the frequencies of hypo-CO (blue) and hyper-CO (orange) nuclei is defined as the variability index (VI), determined from the data (left) and the corresponding normal distributions (right; Figure S2A).

(E and G, left) Comparisons as in (B) for COs in the five indicated organisms. **Female data come from DNA sequencing.

(F and G, right) Comparisons as in (B), (D), and (E) for early intermediates in the two indicated organisms. ##Data are available only for chromosomes 13, 14, 15, 21, and 22.

Data sources and details of statistical analysis are given in STAR Methods. For human male, Sordaria, tomato, tiger, elephant shrew, and human female at CO stages, and human male and Sordaria at early intermediate stages, n = 755, 94, 111, 59, 63, 69, 36, and 26, respectively. Error bars indicate SD (B, E, and F) or SE (D and G). See also Figures S1, S2, and S3.

indicator of the magnitude of this effect. These various effects are observed for nuclei from several different individuals, indicating that they are a common general feature of human male meiosis (Figures S1E and S1F).

The same overdispersion seen in human male is observed in several other organisms as defined by CO focus data for two other mammals (tiger and elephant shrew), the higher plant tomato, and the filamentous fungus Sordaria, and by DNA sequence data for "meiotic tetrads" in human female (Figures 1E, 1G, and S2A). All datasets exhibit: (1) a significantly higher CV for total COs per nucleus in experimental data as compared to those predicted for the hypothesis of independence from *in silico* nuclei; (2) VIs ranging from 20% to 50%; and (3) roughly equal numbers of hyper- and hypo-CO nuclei. These effects thus appear to be an evolutionarily conserved feature of the basic meiotic program.

Per-Nucleus Covariation of COs

Overdispersion in the distribution of COs per nucleus directly implies that the numbers of COs on different chromosomes tend to

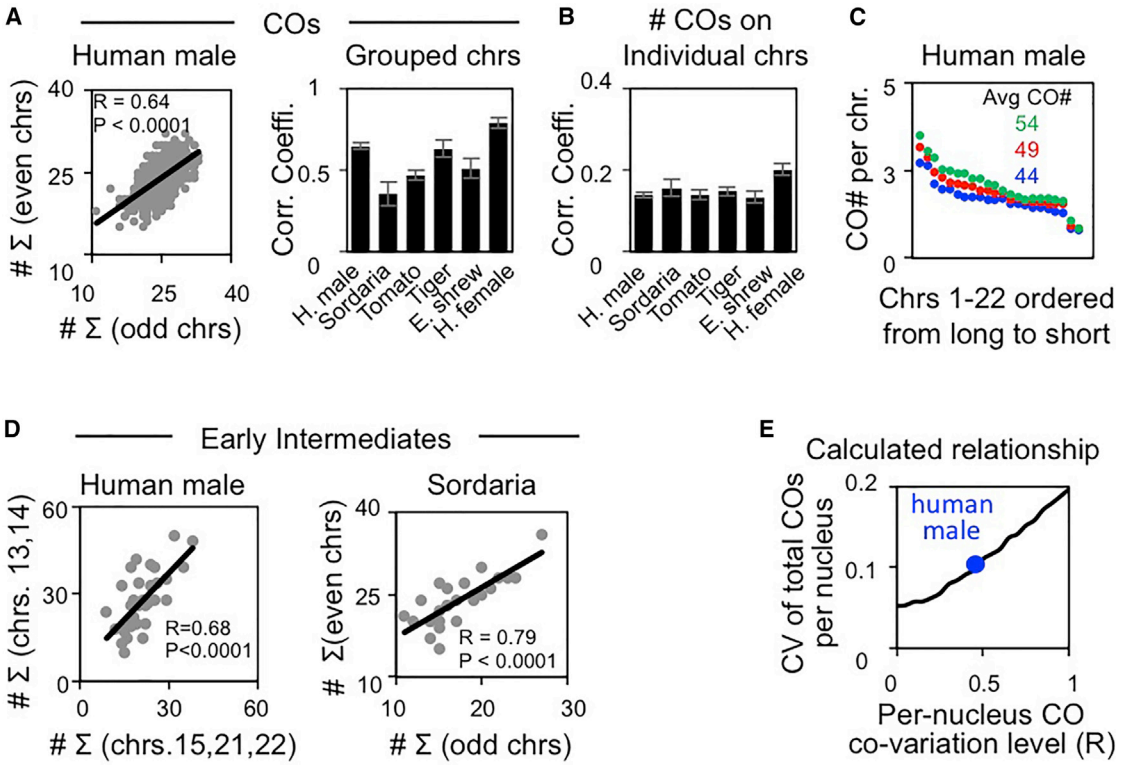

Figure 2. Experimental Documentation of per-Nucleus Covariation of COs

(A and B) For the six organisms analyzed for COs in Figure 1, the numbers of CO foci in single individual nuclei are correlated for two matched groups of chromosomes (e.g., odd versus even chromosomes in A, left) and on pairs of individual chromosomes for all possible combinations (B).

(C) Human male nuclei with high, medium, and low total CO numbers exhibit the same hierarchy for all 22 autosomes.

(D) For the two organisms analyzed for early intermediates in Figure 1, the numbers of early intermediate foci in single individual nuclei are correlated for two matched groups of chromosomes.

(E) Simulations (STAR Methods) confirm that stronger per-nucleus covariation of COs gives increased variation in the total number of COs per nucleus (defined by CV). Sample sizes as in Figure 1. Error bars = SE (A, right, and B). Data sources and details of statistical analysis are given in STAR Methods.

See also Figures S1 and S2.

covary, at higher or lower levels, within individual nuclei (Equation 1 in Table 1). This tendency for covariation can be observed experimentally. If chromosomes of an experimental sample are divided into two comparable groups, e.g., odd-numbered and even-numbered autosomes (STAR Methods), the numbers of events on bivalents in the two groups are seen to be correlated within individual nuclei (Figure 2A). Per-nucleus correlation is also seen between (1) the numbers of events on two different individual chromosomes (Figure 2B) and (2) the number of events on one bivalent with the number on all other bivalents in the same nucleus (Figure S2B). Accordingly, groups of nuclei exhibiting high, intermediate, or low total numbers of COs exhibit the same hierarchy of CO levels for every chromosome (Figure 2C). Further, for human male, the CV for COs per nucleus and the degree of covariation between odd- and even-numbered chromosomes exhibit exactly the predicted relationship (Figure 2E; STAR Methods).

Covariation Contributes Half or More of the Total Variance in the Number of COs per Nucleus

The total variance of CO number per nucleus ("*A*") can be decomposed mathematically into two sources (Table 1A): the sum of the "intrinsic variance" of CO numbers on each chromosome ("*B*"), and the sum of the covariances of CO numbers across all pairs of distinct chromosomes ("*C*"). Values of *A*, *B*, and *C* can be calculated directly from the experimental data. The proportional contribution of CO covariance to the total variance in CO number is given by the ratio *C*/*A*. All of the per-nucleus CO datasets described above exhibit positive values for total covariance (column *C* in Table 1B-I). Moreover, the contribution of covariation comprises 48%–83% of the total observed variance (*C*/*A* = 0.48–0.83; Table 1B-I) and thus is a major determining factor in all cases. (Note: the observed covariance cannot be due to the fact that every pair of homologs almost always acquires at least one CO [as required to ensure their regular segregation; Introduction] because, mathematically, neither variance nor covariance change when one CO is removed from every bivalent.)

Interestingly, the variation in COs per nucleus is particularly large in human female (e.g., Figure 1E; Table 1B-I). This difference results from the fact that human female meiosis is afflicted by a unique feature, CO maturation inefficiency (CMI), which acts at a late stage in the recombination process

Table 1. Analysis of Variance

A.

$$\underbrace{\mathrm{Var}\left(\sum_{k=1}^{n}\mathrm{CO}_k\right)}_{(A)} = \underbrace{\sum_{k=1}^{n}\mathrm{Var}(\mathrm{CO}_k)}_{(B)} + \underbrace{\sum_{i\neq j}\mathrm{Cov}(\mathrm{CO}_i,\mathrm{CO}_j)}_{(C)} \qquad \text{(Equation 1)}$$

B. Decomposition of CO Variance

Organism	(*A*) = Observed Total Variance	(*B*) = Variance if Independent	(*C*) = Covariance	(*C*/*A*) = Contribution of Covariance to Total Variance	CV
I. COs per nucleus					
H. male	25.3	6.2	19.1	0.75	0.10
Sordaria	8.9	4.6	4.3	0.48	0.13
Tomato	11.3	4.9	6.4	0.57	0.19
Tiger	47.0	13.0	34.0	0.72	0.11
E. shrew	13.3	5.3	8.0	0.60	0.13
H. female[a]	257.0	44.4	212.6	0.83	0.19
II. Early intermediates per nucleus					
H. male[b]	218.4	76.3	142.1	0.65	0.31
Sordaria	62.9	16.1	46.8	0.74	0.19
III. CO stage – axis length per nucleus[c]					
H. male	19,827.1	2,541.3	17,286.4	0.87	0.16
Sordaria	56.9	11.8	45.2	0.79	0.14
Tomato	325.6	36.9	288.7	0.89	0.07
Tiger	164,804.3	13,817.4	150,987.1	0.92	0.14
E. shrew	121,045.2	29,112.1	91,933.3	0.76	0.13
IV. Early intermediate stage – axis length per nucleus					
H. male[b]	196.2	64.7	131.3	0.67	0.17
Sordaria	114.5	26.2	88.4	0.77	0.14
V. COs per gamete					
H. male – sperms[a]	19.4	14.3	5.1	0.26	0.18
H. male sperms – pred. from MLH1	18.7	13.9	4.8	0.26	0.18
H. female – eggs[a]	79.0	28.3	50.7	0.64	0.21
H. female eggs – pred. from tetrads	85.4	32.2	53.2	0.62	0.22

(A) Equation 1: The total variance of CO number in a cell ("*A*") can be decomposed into contributions from the variances for individual chromosomes ("*B*") and the covariances for pairs of chromosomes ("*C*") (STAR Methods). The contribution of cross-chromosome covariance to total variance is *C*/*A*. *n* is the number of bivalents. (B) Values of *A*, *B* and *C* from Equation 1 for all analyzed datasets with respect to (I) COs; (II) Early Intermediates; (III) Axis/SC lengths at the CO stage; (IV) Axis/SC lengths at the early intermediate stage; and (V) COs per gamete.

[a]From DNA sequence data (all other data from recombination foci).

[b]For human male, RPA foci and axis/SC length data are available only for chromosomes 13, 14, 15, 21, and 22.

[c]Female axis lengths at the CO stage are not available because data come from DNA sequence analysis (text).

to effectively "subtract" COs stochastically from the original array set up by CO designation and interference (Wang et al., 2017). Nonetheless, covariance is still the predominant factor in determining total variance (C/A = 83%; Table 1B-I).

These findings are confirmed and extended by analysis of DNA sequence data from post-prophase products of human male and female meiosis (Table 1B-V; STAR Methods). CO patterns in individual sperm exhibit CO covariation, at exactly the level predicted for gametes from MLH1 focus analysis under the assumption of no chromatid interference. This correspondence has three implications. (1) Prophase focus data accurately report final CO numbers. (2) Chromatid interference is either absent or extremely weak in human male, as has been found in other organisms (Zhao et al., 1995; Mancera et al., 2008) and in human female (Hou et al., 2013). (3) Covariation set up at prophase, as seen in MLH1 focus patterns, is maintained essentially unaltered through gamete formation, without any detectable influence of covariation-induced biases in the loss of hypo- or hyper-CO gametes. These conclusions are bolstered by the fact that, for human female, covariation observed in gametes (eggs) is the same as that predicted for

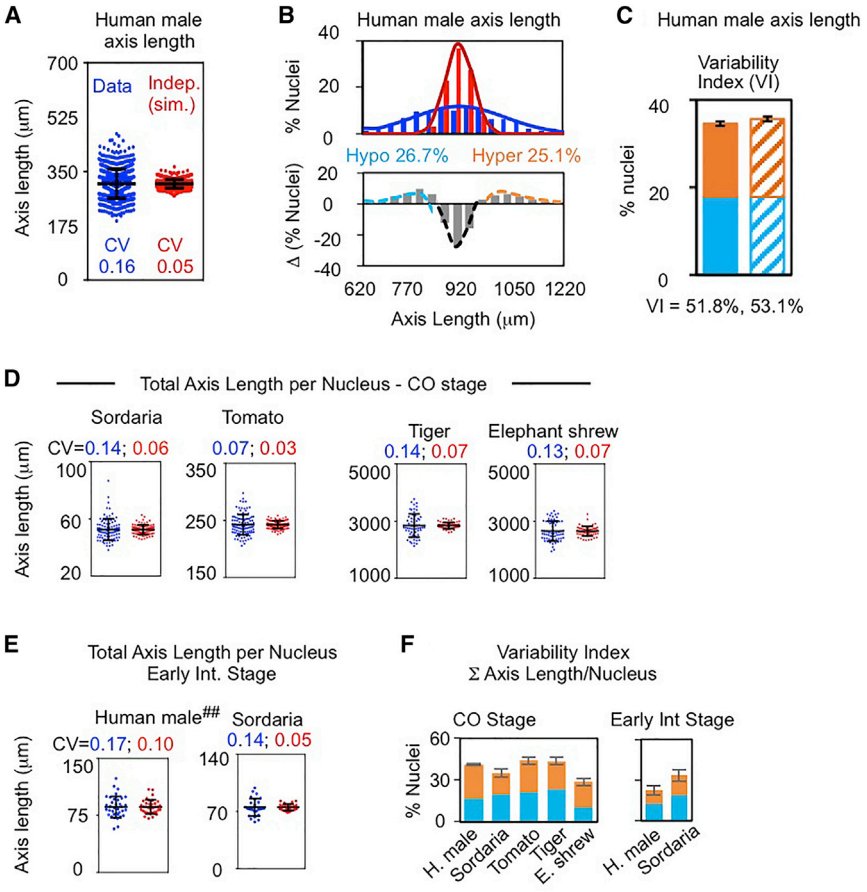

Figure 3. Overdispersed Distribution of Total Axis Lengths per Nucleus

(A)–(F) are exactly analogous to (B)–(G) of Figure 1 except that they pertain to axis lengths at the CO and early intermediate stages rather than the corresponding recombination events. ##Data are available only for chromosomes 13, 14, 15, 21, and 22. Sample sizes as in Figure 1. Error bars, SD (A, D, and E) or SE (C and F).

See also Figures S1 and S2.

gametes from full prophase "tetrads," each reconstituted from an egg plus the associated first and second polar bodies (Table 1B-V). We also note that these findings for human gametes explain the "gamete effect" of Kong et al. (2002, 2014), who observe, in sequenced human pedigrees, that the number of COs transmitted to a given offspring is correlated across chromosomes.

Early Recombination Intermediates Exhibit per-Nucleus Covariation

During meiosis, CO sites are designated (with accompanying CO interference) at early- or mid-prophase from among a much larger array of early recombination interactions, each set up by a corresponding initiating double-strand break (Hunter, 2015). All of the patterns described above for COs are also observed for these early intermediates, as defined by analysis of RPA foci in human male and Hei10 T2 foci in Sordaria, including (1) an overdispersed distribution of total foci per nucleus, with high VI's and roughly equal numbers of hyper- and hypo-focus nuclei (Figures 1F, 1G, S1A, and S1B), (2) per-nucleus correlations in the numbers of foci observed in two equivalent chromosome groups (Figure 2D), and (3) positive levels of total covariance and large contributions of covariance to total variance (Table 1B-II).

Prophase Chromosome Axis Lengths Exhibit per-Nucleus Covariation

Every experimental feature diagnostic of per-nucleus covariation of COs, and of early recombination events, is also observed analogously for bivalent axis (SC) lengths at the corresponding stages. (1) Total axis lengths per nucleus are overdispersed, with high VIs and roughly equal numbers of hyper- and hypo-axis length nuclei (Figures 3, S1G, and S1H). (2) Per-nucleus covariation is seen for axis lengths between different groups of chromosomes or individual chromosomes (Figures 4A, 4B, 4D, and S2D–S2F), or an individual chromosome and a chromosome group (Figure S2C). Accordingly, groups of nuclei exhibiting high, intermediate, or low total axis lengths exhibit the same hierarchy of axis lengths for every chromosome (Figure 4C). (3) Axis lengths at both stages exhibit positive values of total covariance and large contributions of total covariance to total variance (Table 1B-III, IV).

Per-Nucleus Covariation of Prophase Chromosome Axis Lengths Dictates per-Nucleus CO Covariation

The axis length of an individual chromosome determines the number of initiated recombination events (DSBs), total early recombination interactions and, then, interference-mediated COs. Correlations between axis length and event number are documented in several organisms (e.g., human male and female meiosis; Figure 1A; Kleckner et al., 2003; Wang et al., 2017). Moreover, (1) Axis lengths are the same regardless of whether recombination has been initiated, not initiated, or initiated at a reduced level (Storlazzi et al., 2003; Tessé et al., 2003; Zhang et al., 2014a, 2014c; Cole et al., 2012a). (2) Mutations in axis components coordinately alter not only axis length but also CO levels (Novak et al., 2008; Revenkova et al., 2004; Zhang et al., 2014c; Fung et al., 2004; Mets and Meyer, 2009). (3) Human male and female meiosis exhibit, respectively, shorter and longer axes, and fewer and more COs but have identical recombination processes including the density of early recombination interactions per axis length and the parameters governing CO designation and interference (Wang et al., 2017).

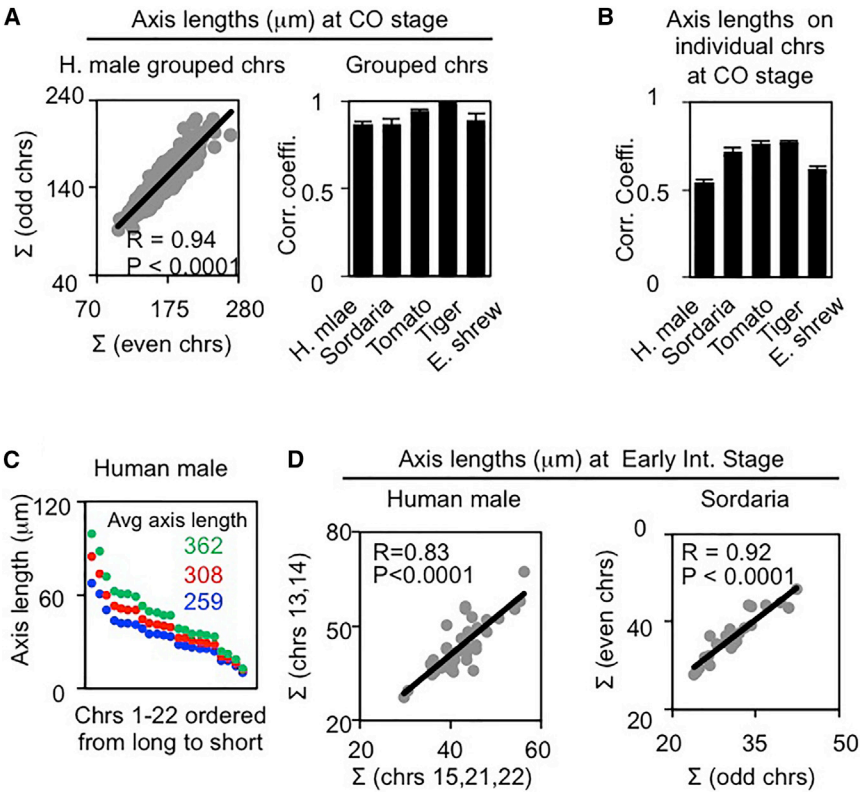

Figure 4. Experimental Documentation of per-Nucleus Covariation of Axis Lengths

(A)–(D) are exactly analogous to (A)–(D) of Figure 2 except that they pertain to axis lengths at the CO and early intermediate stages rather than the corresponding recombination events. Sample sizes are as in Figure 1. Data sources and details of statistical analysis are given in STAR Methods. Error bars, SE (A, right, and B).

See also Figures S1 and S2.

If chromosome axis length determines the average number of COs per bivalent, it follows directly that per-nucleus covariation of axis lengths should determine per-nucleus covariation of COs. In accord with this causality, per-nucleus correlation coefficients for grouped chromosomes and the proportion of total variance resulting from covariation (C/A, above) are both substantially higher for axis lengths than for COs ($R > 0.9$ versus 0.4–0.8; and 76%–92% versus 48%–83%, respectively [Figures 4A and 2A and Table 1B-I, III, respectively]).

Additionally, simulation of recombination patterns shows that per-nucleus covariation of axis lengths can quantitatively explain CO covariation. In previous work, we used this approach to determine, for human male meiosis, the values of all parameters that define the basic features of CO recombination (e.g., the array of total early interactions and the nature of CO site specification by CO designation and interference) (Wang et al., 2017). We have now included in the simulation algorithm two additional parameters that specify (1) intrinsic variation in axis lengths; and (2) covariation among axis lengths of different bivalents in the same nucleus (STAR Methods). When the values of these two parameters are set at the levels defined experimentally (Figures S2C–S2E and S3A; STAR Methods), simulation of human male CO patterns yields a nearly perfect match to experimental data with respect to (1) the CV for the total number of COs per nucleus (Figure 5A, green versus blue), the CV for total COs per nucleus predicted for *in silico* nuclei by the hypothesis of independence (Figure 5A, purple versus red), and the accompanying percentages of hyper- and hypo-CO nuclei and the VI (Figure 5B); (2) the per-nucleus correlation coefficients for COs in odd versus even chromosome groups, for pairs of individual chromosomes, and for individual chromosomes versus a chromosome group (Figure 5C green versus blue); (3) total variance, intrinsic variance, and covariance and, thus the contribution of covariance to total variance, of COs per nucleus; and (4) previously analyzed features (Figure S3B).

Finally, in most organisms, axis lengths are set up early in prophase where they determine not only CO frequencies but the frequencies of total initiating double-strand breaks and of early intermediates, among which a selected subset are CO sites (Zhang et al., 2014b, 2014c; Wang et al., 2017). In accord with this progression, covariation is also observed for early intermediates and their corresponding axis lengths, by all criteria (Figures 1, 2, 3, and 4; Table 1B-III, IV). By implication, (1) covariation will apply also to gene conversion (GC) events, which arise from all types of early intermediates but primarily from those that yield "non-crossover" products (Cole et al., 2012b), and (2) individual nuclei (and gametes) will tend to exhibit especially high or especially low levels coordinately for both GCs and COs.

Per-Nucleus CO Covariation Aids Evolutionary Adaptation in a Sporadically Fluctuating Environment

Per-nucleus CO covariation has the effect of increasing the proportions of gametes with extremely low and with extremely high CO numbers (above). During sexual reproduction, gametes with few COs tend to lead to offspring that are phenotypically similar to their parents, while gametes with many COs lead to offspring with substantial phenotypic variation. CO covariation, by elevating hypo-CO and hyper-CO gametes, concomitantly increases the proportions of both of these classes of offspring. At the same time, by reducing the proportion of mid-CO gametes, it reduces the number of offspring whose phenotypes are intermediately different from their parents' (Figure 6A). The effect of CO covariation on CO levels in gametes is thus expected to have significant consequences for the fitness of the resulting offspring according to the environment(s) in which they find themselves.

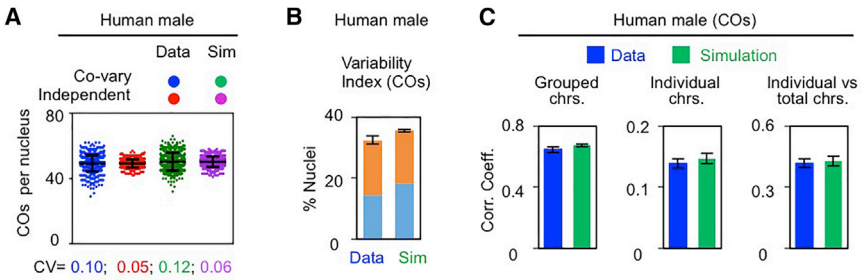

Figure 5. Simulation Analysis Shows that Intrinsic Variation and Covariation of Axis Lengths Can Quantitatively Explain per-Nucleus Covariation of COs in Human Male

(A–C) Recombination event patterns were predicted by an enhanced simulation analysis that parameterizes both intrinsic variation and covariation of chromosome axis lengths (text; STAR Methods). For human male COs, simulation using the experimentally defined values for both of these parameters perfectly predicts all experimentally observed features including the CV of total COs per nucleus (A, green versus blue) and the three per-nucleus correlations in CO numbers on grouped and/or individual chromosomes as described in Figures 2A, 2B, and S2B (C, green versus blue). Moreover, simulation using the experimentally defined axis variation but zero axis-length covariation perfectly predicts the outcome of the "hypothesis of independence" (text) (A, purple versus red). Correspondingly, predicted levels of hyper-CO (orange) and hypo-CO (blue) nuclei and the corresponding VI exactly match those defined from experimental data (B). Data sources and details of statistical analysis are given in STAR Methods. Error bars, SD (A) or SE (B and C).
See also Figures S1, S2, and S3.

Covariation Is Predicted to Confer an Advantage in a Fluctuating Environment

One circumstance in which CO covariation could potentially confer an advantage is where a species experiences occasional fluctuations in its environment, across time or space. Such environmental fluctuations, either biotic or abiotic, are faced by the majority of species (Williams, 1975). If the environment does not change between a parental generation and an offspring generation, then selection will tend to favor offspring that are similar to their parents, whose phenotypes (and perhaps those of *their* parents, etc.) were tried and tested in the same environment (Figure 6B). In this situation, the fittest offspring are likely to be enriched for those produced from hypo-CO gametes (Figure 6A); this will favor parents whose gametes exhibited CO covariation. If, instead, the environment changes between the parental and offspring generations, then selection will shift to favoring a phenotype different from that favored in the parental generation and thus can favor new genetic combinations produced by crossing over. If the environmental shift is large, the fittest offspring will tend to be enriched for those with many new genetic combinations (Figure 6C). This again will favor parents who exhibited CO covariation, due to their elevated levels of hyper-CO gametes (Figure 6A). This selection for hyper-CO gametes will be stronger, the more severe the environmental change. Only in the case where the environmental changes, but the change is mild, can mid-CO gametes be favored (Figure 6D), and, thus, CO covariation disfavored (Figure 6A).

Population Genetic Modeling Defines the Advantage of Covariation in a Fluctuating Environment

To investigate the above logic more formally, we have constructed a minimal population genetic model of selection in a fluctuating environment (full details in STAR Methods). For convenience, the model organism is a unisexual haploid, and sexual reproduction occurs by the fusion of two individuals, followed by meiosis. To allow for CO covariation across chromosomes, four loci are considered—one pair of loci on each of two different chromosomes—with alleles A/a and B/b, and C/c and D/d, respectively. In a given generation, there is a favored combination of alleles on each chromosome: e.g., AB and ab on chromosome 1, and CD and cd on chromosome 2. (This symmetry—e.g., if aB is favored then so is Ab—ensures that polymorphism is maintained at all loci, and thus allows us to focus directly on the effect of recombination without having to worry about drastic swings in the frequencies of particular alleles (e.g., Charlesworth, 1976; Sasaki and Iwasa, 1987)). The favored combination of alleles remains constant in periods of environmental stasis and changes to a different combination after the environment changes.

Our general strategy was to simulate separately and then compare the evolutionary dynamics of a population that exhibits no CO covariation between the two locus pairs and of a population that does exhibit CO covariation (full recursion equations provided in STAR Methods). In each simulation, we calculated the average growth rate (geometric mean fitness) of the population across 10^7 generations. For a given comparison, if the population employing CO covariation has a higher average growth rate than the population employing no CO covariation, we expect that CO covariation would usually outcompete no covariation in a population mixed for the two strategies (Karlin and McGregor, 1974).

Simulations were carried out over a range of values of five specified parameters. (1) A baseline rate of recombination between each locus pair, r. This rate is chosen arbitrarily, recognizing that the recombination rate between each locus pair could have evolved for reasons other than, or in addition to, environmental fluctuations (e.g., alleviation of Hill-Robertson interference). (2) The level of covariation of COs at the two locus pairs, K, which ranges from 0 (no covariation) to 1 (maximal covariation). (3) The average period of environmental fluctuations, T generations. Specifically, in each generation, there is a probability $1/T$ that the environment changes. (4) The probability p that, when the environment does change, the newly favored allele combination changes on both chromosomes (e.g., from AB/ab and CD/cd to Ab/aB and Cd/cD). $1 - p$ is then the probability that the newly favored allele combination changes on only one of the two chromosomes (each equally likely). (5) The strength of selection, s, defined as the relative selective advantage of the fittest genotype over the least fit genotype.

We focused primarily on a selection scenario where only those offspring that are best genetically equipped for their environment are likely to survive and reproduce. This scenario applies to the majority of extant species, and likely also to those ancestral species in

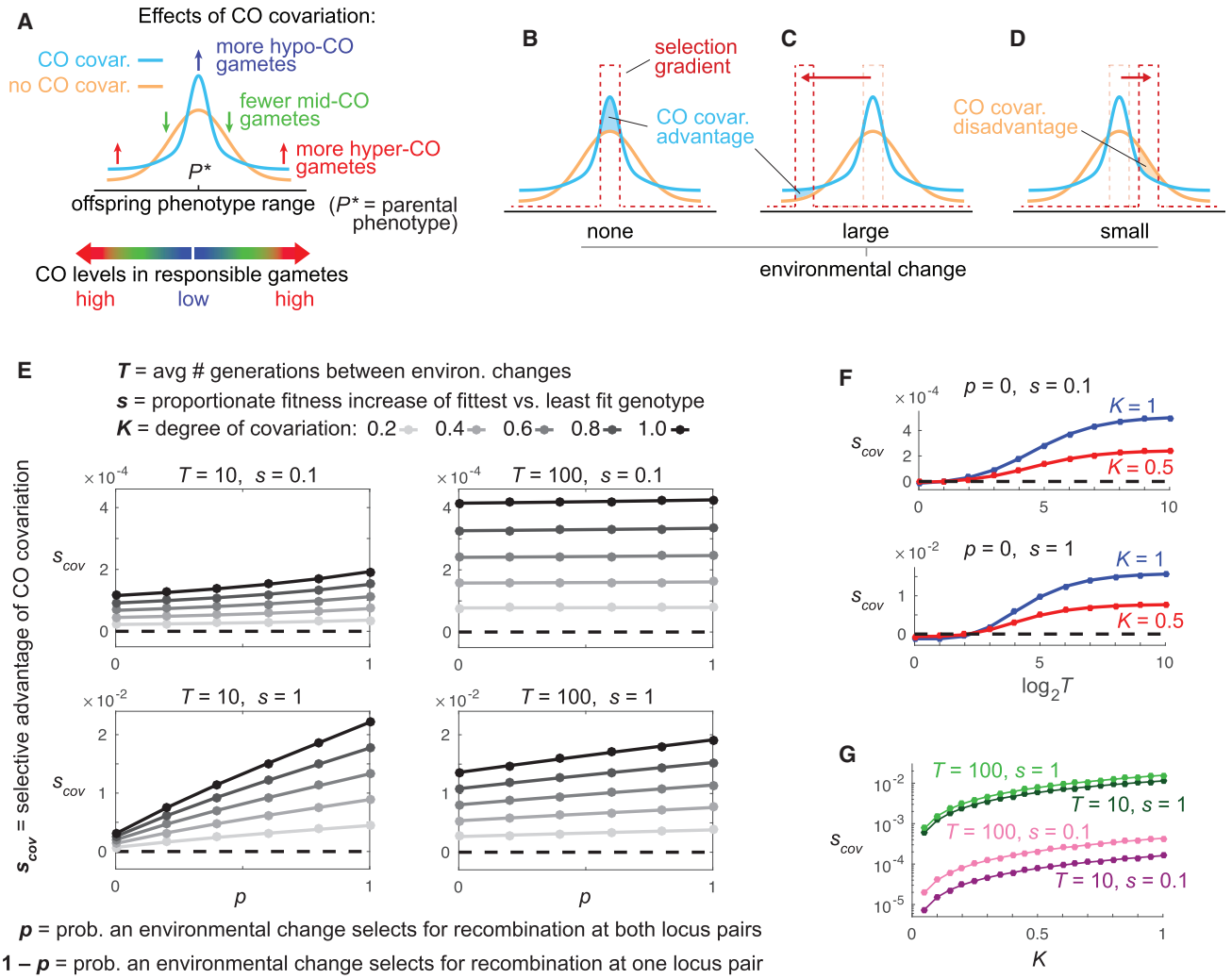

Figure 6. Mathematical Modeling Demonstrates the Evolutionary Advantage of Crossover Covariation

(A) CO covariation causes an overproduction of hypo-CO and hyper-CO gametes, which, respectively, increase the frequencies of offspring with trait values very close to, and very far from, the parental value.

(B) When the environment does not change, offspring with trait values near the parental value are favored, and thus covariation is favored.

(C) When the environment changes substantially, offspring with trait values far from the parental value become favored, and thus covariation is again favored.

(D) Only when the environment changes a little is covariation disfavored.

(E) The selective advantage of covariation is revealed formally in a four locus population genetic model with a fluctuating environment. CO covariation enjoys a selective advantage in all scenarios. The selective advantage of covariation increases with p, the probability that each environmental change favors hyper-CO gametes with COs between both locus pairs. However, covariation is favored even when $p = 0$, so that environmental changes always favor gametes with a CO between only one locus pair, and thus always disfavor covariation. Here, the benefit of covariation derives from its overproduction of hypo-CO gametes in the periods of stasis between environmental changes.

(F) Consistent with this logic, when $p = 0$, the advantage of covariation grows as the average period of stasis, T, grows.

(G) The advantage to covariation increases monotonically with the degree of covariation.

See also Figures S4, S5, and S6.

which the basic features of sex and recombination evolved (Williams, 1975). In this case, across a wide range of parameter specifications, the population employing CO covariation virtually always enjoys a higher average growth rate than the population without CO covariation. Moreover, the advantage of covariation increases as the degree of covariation increases (Figure 6E, grayscale; Figures 6F, red versus blue; Figures 6G and S4C). These findings provide a proof of principle that CO covariation can be evolutionarily advantageous in populations faced with fluctuating environments. We obtain similar results when selection is more even across genotypes (multiplicative across chromosomes) (Figure S5). However, in the opposite case to that we have focused on, where selection acts so that all but the very least fit reproduce, the results are more equivocal, with CO covariation sometimes being advantageous, and sometimes not (Figure S6).

Additional findings support our specific prediction that the advantage of covariation derives from its elevation of both hyper- and hypo-CO gametes, due to their different advantages in changed or static conditions, respectively. Consistent with this, (1) the advantage of CO covariation tends to be larger when environmental shifts more often alter the favored genetic combinations at both locus pairs; i.e., when p is larger (Figures 6E and S4A). Intuitively, this can be understood as the case where environmental changes are often large (Figure 6C), with the positive effects of covariation in creating new combinations coordinately on two (or more) chromosomes resulting from elevation of hyper-CO gametes (Figure 6A). (2) However: the advantage of CO covariation is also apparent at low values of p (Figure 6E). In the extreme case of $p = 0$, a change in the environment always favors recombination at only one locus pair. Intuitively, this corresponds to the case where environmental shifts are always small (Figure 6D). In this case, environmental changes always disfavor CO covariation because small environmental shifts select for mid-CO gametes (in our model, 1 CO; Figures 6A and 6D). Therefore, we infer that covariation's advantage in the case of small p must derive from a benefit conferred in the periods of stasis between environmental changes, and, specifically, from overproduction of hypo-CO gametes in these periods (Figures 6A and 6B). This interpretation is directly supported by an additional finding: when $p = 0$, the advantage of CO covariation is typically greater if the average period of stasis between environmental changes, T, is longer (Figures 6F and S4B).

To more comprehensively study the effects of the various parameters on the evolutionary success of CO covariation, we focused on a simple specification of the model where, when the environment changes, a new set of favored alleles is selected, with all of the alternative combinations being equally likely. Under this specification, we find again that CO covariation typically improves the average population growth rate relative to no CO covariation. The size of this advantage (1) is monotonic in the degree of CO covariation (Figures 6G and S4C); (2) tends to increase with the average period between environmental changes, T, unless selection is very strong (Figure S4D); and (3) increases with the strength of selection (Figure S4E).

DISCUSSION

Here, we identify a fundamental new feature of meiotic recombination: per-nucleus CO covariation. This feature is evolutionarily conserved, as seen by documentation in three mammals, a higher plant, and a fungus. The existence of per-nucleus CO covariation raises two general questions. What is the mechanism? And what is its significance? We have begun to provide answers to both questions.

Mechanism

We show that the proximate basis for per-nucleus covariation of COs is analogous per-nucleus covariation of chromosome axis lengths. This conclusion is concordant with, and a direct extension of, diverse evidences that chromosome axis length determines CO number, as documented above. What could determine CO axis length? It has been shown that the density of chromatin loops along prophase chromosome axes is evolutionarily conserved (Kleckner, 2006). This feature, in turn, directly implies that axis length and chromatin loop length are inversely related. Correspondingly, longer/shorter axes in correlation with shorter or longer loops have been documented in a number of situations: in the two sexes of a given organism (including human) (Gruhn et al., 2013; Tease and Hultén, 2004), domainally in heterochromatin versus euchromatin in tomato (e.g., Stack et al., 2009), and in the PAR region of mammalian X and Y chromosomes (Kauppi et al., 2011). Further, in mouse, deletion of a single meiotic axis component, *smc1β*, is sufficient to confer shorter chromosome axes and correspondingly larger chromatin loops (Novak et al., 2008; Revenkova et al., 2004). These observations imply that global modulation of loop length is a general mechanism for determining chromosome axis length and, therefore, the number of COs per chromosome (see discussion in Wang et al., 2017). Thus, in the present case, per-nucleus covariation of CO numbers could be a natural consequence of global determination of chromatin loop size.

Significance for Evolution

The distribution of total COs per nucleus, as observed experimentally, is significantly broader than that predicted if CO numbers were specified independently on different chromosomes, and this difference is driven by covariation of CO number across chromosomes within nuclei. As a direct consequence, CO covariation significantly increases the frequencies of nuclei (and thus gametes) that have especially high or especially low levels of COs, coordinately on all chromosomes. We reasoned that this feature might increase the ability of COs to promote evolutionary adaptation: on the one hand, hyper-CO gametes would be available when new genetic combinations are needed for adaptation; on the other hand, hypo-CO gametes would be available when it is more advantageous to retain ancestral, well-evolved combinations. The question then arises: in which specific situation(s) would the increased availability of these two types of gametes confer a selective advantage?

We further reasoned that covariation could be advantageous in a fluctuating environment. More hyper-CO gametes would be available for times of environmental change, when new genetic combinations become favored, and more hypo-CO would be available for periods of stasis, when the environment is not changing and creation of new combinations by crossing over would tend to be deleterious. Population genetic modeling provides support for the validity of these predictions. In scenarios where environmental changes are separated by periods of stasis, covariation significantly increases mean fitness, in proportion to the degree of covariation, and over a wide range of parameter specifications. Moreover, details of the observed effects provide specific evidence that covariation is favorable via its elevations of both hyper-CO and hypo-CO gametes (above).

This analysis provides an initial proof of principle that CO covariation can be advantageous in fluctuating environments, as probably faced by all species (Williams, 1975). If so, CO covariation expands the power of meiotic recombination to promote evolutionary adaptation. We note that while our evolutionary argument suggests an adaptive advantage of CO covariation via its effect on the variance of CO number across gametes, it applies more broadly to any source of such variance. It

therefore suggests a general evolutionary explanation for the substantial intra-individual variance in CO number observed in many species (e.g., Ruiz-Herrera et al., 2017; Wang et al., 2017).

COs have diverse roles in adaptation, whose relative contributions to the evolutionary maintenance of recombination are much debated (e.g., Felsenstein, 1974; Williams, 1975; Maynard Smith, 1978; Bell, 1982; Barton, 1995; Barton and Charlesworth, 1998; Otto, 2009). Importantly, by the logic above, CO covariation will aid in the response to environmental fluctuations even if other factors are the predominant reasons for the maintenance of COs. We note, however, that the model we employed is, by necessity, highly simplified, ignoring a number of biological complexities that could plausibly affect the degree to which CO covariation is advantageous, e.g., analysis of only four loci, inclusion of only two chromosomes, and a limited number of environmental fluctuation regimes (STAR Methods). In addition, a more direct demonstration of the advantage of CO covariation in our model would involve competing alleles at a fifth, unlinked "modifier" locus, the alleles at which have no direct effect on fitness but influence the level of CO covariation among the other four loci. Future studies can address these complexities.

We also note that Hadany and Beker (2003) argue that it is favorable for low-fitness individuals to recombine their genomes substantially, but not for high-fitness individuals to do so. Such "fitness associated recombination" is directly apparent when high recombination is induced by, or associated with, environmental change (Introduction) but is also mirrored in the situation described here, where environmental change reduces the fitness of currently common genotypes while environmental stasis maintains the fitness dominance of common genotypes.

Additional advantages of CO covariation can also be considered. First, we note that chromosomes lacking even a single CO are prone to mis-segregation (Zickler and Kleckner, 1999). CO covariation does not confer an overall increase in the frequency of chromosomes lacking a CO, which is a function of the basic mechanism by which meiotic CO patterns are determined (Zhang et al., 2014b, 2014c; White et al., 2017). However, it does tend to bundle zero-CO chromosomes into a smaller fraction of nuclei (e.g., Wang et al., 2017) and will thereby decrease the overall probability that a nucleus will exhibit aberrant segregation(s) at Meiosis I. This effect, while small, represents an effective additional benefit of covariation.

Second, while we have focused here on scenarios involving short-term effects of recombination in a fluctuating environment, it is not impossible that CO covariation might also be beneficial for longer-term evolution, even in stable environments. Laboratory evolution experiments show that, under constant environmental conditions, population fitness increases over time, seemingly without bound, as new beneficial mutations (and combinations of mutations) continually arise and are incorporated (e.g., Wiser et al., 2013). In this case, it is the "allelic environment" of the organism that is constantly changing over time. Correspondingly, it is possible that, in some regimes, in the presence of covariation, hyper-CO gametes will increase the rates at which independently arising favorable mutations become linked and favorable mutations become separated from linked deleterious ones (Introduction), whereas hypo-CO gametes will keep new mutations together once they have become linked.

Third, when DNA is introgressed, via hybridization, from the genome of one species into another's, introgressed genes that are incompatible with the recipient genome are purged by purifying selection. This process also removes introgressed DNA surrounding the incompatible genes, with larger blocks removed in regions of low recombination. Higher recombination thus causes finer "trimming," allowing greater retention of introgressed DNA that is neutral or beneficial (Brandvain et al., 2014; Schumer et al., 2018; Edelman et al., 2018; Martin et al., 2019). Introgression and purging, like CO covariation, are genome-wide events, and the timescale of purging is short—on the order of a few generations (Harris and Nielsen 2016; Schumer et al., 2018). After a pulse of introgression, hypo-CO gametes are expected to be favorable if there are many incompatible genes and few beneficial genes in the introgressed DNA, since hypo-CO gametes allow rapid purging of many large blocks of introgressed DNA. Under this scenario, CO covariation would speed the purging of incompatibilities by providing an excess of hypo-CO gametes. If, on the other hand, introgressed DNA harbors many beneficial new genes, then hyper-CO gametes will be favorable in rapidly unlinking these beneficial genes from linked incompatible genes, so that a greater number of beneficial genes can be retained in the recipient species' genome.

We also note that CO covariation is of general significance for population genetic modeling. Classic population models that probe the evolutionary advantages of recombination mostly involve only two loci, although multi-locus models have been developed to understand genomic evolution and the evolution of recombination (e.g., Hamilton et al., 1990; Charlesworth et al., 1993; Barton, 1995; Lenormand, 2003; Otto and Nuismer, 2004). Since CO covariation appears to be conserved across eukaryotes, future multi-locus population genetic models must take this phenomenon into account if they are to be empirically realistic.

STAR★METHODS

Detailed methods are provided in the online version of this paper and include the following:

- KEY RESOURCES TABLE
- EXPERIMENTAL MODEL AND SUBJECT DETAILS
- CONTACT FOR REAGENT AND RESOURCE SHARING
- METHOD DETAILS
  - Data acquisition
  - Co-variation analysis
  - Coefficient of variation analysis
  - Variability index analysis
  - Sorting bivalents randomly into single nuclei
  - Best-fit simulations for CO patterns
  - Predicting CO numbers in gametes
  - Decomposing total variance of COs per nucleus
  - Population Genetic Modeling
- QUANTIFICATION AND STATISTICAL ANALYSIS
  - Details of Statistical Analyses
- DATA AND SOFTWARE AVAILABILITY
  - Software availability

SUPPLEMENTAL INFORMATION

Supplemental Information can be found with this article online at https://doi.org/10.1016/j.cell.2019.02.021.

ACKNOWLEDGMENTS

We thank Brian Charlesworth, Nate Edelman, David Haig, and Matthew Meselson for suggestions and comments on this manuscript. This work, S.W., Y.S., and L.Z. were supported by National Key Research & Development Program of China (2018YFC1003400 and 2018YFC1003700), National Natural Science Foundation of China (projects 31671293 and 31771385), and Taishan Scholars Youth Project of Shandong Province and Shandong Provincial Natural Science Foundation of China (Project JQ201605). C.V. was supported by a stipend from the Department of Organismic and Evolutionary Biology and the Program for Evolutionary Dynamics, Harvard University. This work was also supported by grants to N.K. and D.Z. (NIH RO1 GM044794), D.Z. (Unité Mixte de Recherche 8621, now I2BC), F.S. (National Key Research and Development Program of China, 2018YFC1003500, National Natural Science Foundation of China, 81430027), and A.R.-H. (CGL2014-54317-P, CGL2017-83802-P, and BFU2015-71786-REDT).

AUTHOR CONTRIBUTIONS

S.W., L.Z., C.V., and N.K. analyzed the data and wrote the paper. F.S., A.R.-H., and D.Z. provided data. C.V. constructed and simulated the population genetic model. S.W. and L.Z. did all simulations of CO patterns. All authors contributed to editing the manuscript.

DECLARATION OF INTERESTS

The authors declare no competing interests.

Received: May 16, 2018
Revised: December 17, 2018
Accepted: February 13, 2019
Published: March 14, 2019

REFERENCES

Anderson, L.K., Lohmiller, L.D., Tang, X., Hammond, D.B., Javernick, L., Shearer, L., Basu-Roy, S., Martin, O.C., and Falque, M. (2014). Combined fluorescent and electron microscopic imaging unveils the specific properties of two classes of meiotic crossovers. Proc. Natl. Acad. Sci. USA *111*, 13415–13420.

Barton, N.H. (1995). A general model for the evolution of recombination. Genet. Res. *65*, 123–145.

Barton, N.H., and Charlesworth, B. (1998). Why sex and recombination? Science *281*, 1986–1990.

Bell, G. (1982). The Masterpiece of Nature: The Evolution and Genetics of Sexuality (University of California Press).

Brandvain, Y., Kenney, A.M., Flagel, L., Coop, G., and Sweigart, A.L. (2014). Speciation and introgression between *Mimulus nasutus* and *Mimulus guttatus*. PLoS Genet. *10*, e1004410.

Charlesworth, B. (1976). Recombination modification in a fluctuating environment. Genetics *83*, 181–195.

Charlesworth, B., Morgan, M.T., and Charlesworth, D. (1993). The effect of deleterious mutations on neutral molecular variation. Genetics *134*, 1289–1303.

Cole, F., Kauppi, L., Lange, J., Roig, I., Wang, R., Keeney, S., and Jasin, M. (2012a). Homeostatic control of recombination is implemented progressively in mouse meiosis. Nat. Cell Biol. *14*, 424–430.

Cole, F., Keeney, S., and Jasin, M. (2012b). Preaching about the converted: how meiotic gene conversion influences genomic diversity. Ann. N Y Acad. Sci. *1267*, 95–102.

De Muyt, A., Zhang, L., Piolot, T., Kleckner, N., Espagne, E., and Zickler, D. (2014). E3 ligase Hei10: a multifaceted structure-based signaling molecule with roles within and beyond meiosis. Genes Dev. *28*, 1111–1123.

Edelman, N.B., Frandsen, P., Miyagi, M., Clavijo, B.J., Davey, J., Dikow, R., Accinelli, G.G., Van Belleghem, S., Patterson, N.J., Neafsey, D.E., et al. (2018). Genomic architecture and introgression shape a butterfly radiation. bioRxiv. https://doi.org/10.1101/466292.

Felsenstein, J. (1974). The evolutionary advantage of recombination. Genetics *78*, 737–756.

Fung, J.C., Rockmill, B., Odell, M., and Roeder, G.S. (2004). Imposition of crossover interference through the nonrandom distribution of synapsis initiation complexes. Cell *116*, 795–802.

Gruhn, J.R., Rubio, C., Broman, K.W., Hunt, P.A., and Hassold, T. (2013). Cytological studies of human meiosis: sex-specific differences in recombination originate at, or prior to, establishment of double-strand breaks. PLoS ONE *8*, e85075.

Hadany, L., and Beker, T. (2003). On the evolutionary advantage of fitness-associated recombination. Genetics *165*, 2167–2179.

Hamilton, W.D., Axelrod, R., and Tanese, R. (1990). Sexual reproduction as an adaptation to resist parasites (a review). Proc. Natl. Acad. Sci. USA *87*, 3566–3573.

Harris, K., and Nielsen, R. (2016). The genetic cost of Neanderthal introgression. Genetics *203*, 881–891.

Hill, W.G., and Robertson, A. (1966). The effect of linkage on limits to artificial selection. Genet. Res. *8*, 269–294.

Hou, Y., Fan, W., Yan, L., Li, R., Lian, Y., Huang, J., Li, J., Xu, L., Tang, F., Xie, X.S., and Qiao, J. (2013). Genome analyses of single human oocytes. Cell *155*, 1492–1506.

Hunter, N. (2015). Meiotic recombination: the essence of heredity. Cold Spring Harb. Perspect. Biol. *7*, a016618.

Jones, G.H., and Franklin, F.C. (2006). Meiotic crossing-over: obligation and interference. Cell *126*, 246–248.

Karlin, S., and McGregor, J. (1974). Towards a theory of the evolution of modifier genes. Theor. Popul. Biol. *5*, 59–103.

Kauppi, L., Barchi, M., Baudat, F., Romanienko, P.J., Keeney, S., and Jasin, M. (2011). Distinct properties of the XY pseudoautosomal region crucial for male meiosis. Science *331*, 916–920.

Kleckner, N. (2006). Chiasma formation: chromatin/axis interplay and the role(s) of the synaptonemal complex. Chromosoma *115*, 175–194.

Kleckner, N., Storlazzi, A., and Zickler, D. (2003). Coordinate variation in meiotic pachytene SC length and total crossover/chiasma frequency under conditions of constant DNA length. Trends Genet. *19*, 623–628.

Kleckner, N., Zickler, D., Jones, G.H., Dekker, J., Padmore, R., Henle, J., and Hutchinson, J. (2004). A mechanical basis for chromosome function. Proc. Natl. Acad. Sci. USA *101*, 12592–12597.

Kong, A., Gudbjartsson, D.F., Sainz, J., Jonsdottir, G.M., Gudjonsson, S.A., Richardsson, B., Sigurdardottir, S., Barnard, J., Hallbeck, B., Masson, G., et al. (2002). A high-resolution recombination map of the human genome. Nat. Genet. *31*, 241–247.

Kong, A., Thorleifsson, G., Frigge, M.L., Masson, G., Gudbjartsson, D.F., Villemoes, R., Magnusdottir, E., Olafsdottir, S.B., Thorsteinsdottir, U., and Stefansson, K. (2014). Common and low-frequency variants associated with genome-wide recombination rate. Nat. Genet. *46*, 11–16.

Laurie, D.A., and Hultén, M.A. (1985). Further studies on bivalent chiasma frequency in human males with normal karyotypes. Ann. Hum. Genet. *49*, 189–201.

Lenormand, T. (2003). The evolution of sex dimorphism in recombination. Genetics *163*, 811–822.

Lhuissier, F.G., Offenberg, H.H., Wittich, P.E., Vischer, N.O., and Heyting, C. (2007). The mismatch repair protein MLH1 marks a subset of strongly interfering crossovers in tomato. Plant Cell *19*, 862–876.

Lian, J., Yin, Y., Oliver-Bonet, M., Liehr, T., Ko, E., Turek, P., Sun, F., and Martin, R.H. (2008). Variation in crossover interference levels on individual chromosomes from human males. Hum. Mol. Genet. *17*, 2583–2594.

Lu, S., Zong, C., Fan, W., Yang, M., Li, J., Chapman, A.R., Zhu, P., Hu, X., Xu, L., Yan, L., et al. (2012). Probing meiotic recombination and aneuploidy of single sperm cells by whole-genome sequencing. Science *338*, 1627–1630.

Lynn, A., Ashley, T., and Hassold, T. (2004). Variation in human meiotic recombination. Annu. Rev. Genomics Hum. Genet. *5*, 317–349.

Mancera, E., Bourgon, R., Brozzi, A., Huber, W., and Steinmetz, L.M. (2008). High-resolution mapping of meiotic crossovers and non-crossovers in yeast. Nature *454*, 479–485.

Marcon, E., and Moens, P. (2003). MLH1p and MLH3p localize to precociously induced chiasmata of okadaic-acid-treated mouse spermatocytes. Genetics *165*, 2283–2287.

Martin, S.H., Davey, J., Salazar, C., and Jiggins, C. (2019). Recombination rate variation shapes barriers to introgression across butterfly genomes. PLoS Biology *17*, e2006288.

Maynard Smith, J. (1978). The Evolution of Sex (Cambridge University Press).

McDonald, M.J., Rice, D.P., and Desai, M.M. (2016). Sex speeds adaptation by altering the dynamics of molecular evolution. Nature *531*, 233–236.

Mets, D.G., and Meyer, B.J. (2009). Condensins regulate meiotic DNA break distribution, thus crossover frequency, by controlling chromosome structure. Cell *139*, 73–86.

Novak, I., Wang, H., Revenkova, E., Jessberger, R., Scherthan, H., and Höög, C. (2008). Cohesin Smc1β determines meiotic chromatin axis loop organization. J. Cell Biol. *180*, 83–90.

Oliver-Bonet, M., Campillo, M., Turek, P.J., Ko, E., and Martin, R.H. (2007). Analysis of replication protein A (RPA) in human spermatogenesis. Mol. Hum. Reprod. *13*, 837–844.

Otto, S.P. (2009). The evolutionary enigma of sex. Am. Nat. *174* (*Suppl 1*), S1–S14.

Otto, S.P., and Nuismer, S.L. (2004). Species interactions and the evolution of sex. Science *304*, 1018–1020.

Ottolini, C.S., Newnham, L., Capalbo, A., Natesan, S.A., Joshi, H.A., Cimadomo, D., Griffin, D.K., Sage, K., Summers, M.C., Thornhill, A.R., et al. (2015). Genome-wide maps of recombination and chromosome segregation in human oocytes and embryos show selection for maternal recombination rates. Nat. Genet. *47*, 727–735.

Revenkova, E., Eijpe, M., Heyting, C., Hodges, C.A., Hunt, P.A., Liebe, B., Scherthan, H., and Jessberger, R. (2004). Cohesin SMC1β is required for meiotic chromosome dynamics, sister chromatid cohesion and DNA recombination. Nat. Cell Biol. *6*, 555–562.

Ruiz-Herrera, A., Vozdova, M., Fernández, J., Sebestova, H., Capilla, L., Frohlich, J., Vara, C., Hernández-Marsal, A., Sipek, J., Robinson, T.J., and Rubes, J. (2017). Recombination correlates with synaptonemal complex length and chromatin loop size in bovids-insights into mammalian meiotic chromosomal organization. Chromosoma *126*, 615–631.

Sasaki, A., and Iwasa, Y. (1987). Optimal recombination rate in fluctuating environments. Genetics *115*, 377–388.

Schumer, M., Xu, C., Powell, D.L., Durvasula, A., Skov, L., Holland, C., Blazier, J.C., Sankararaman, S., Andolfatto, P., Rosenthal, G.G., and Przeworski, M. (2018). Natural selection interacts with recombination to shape the evolution of hybrid genomes. Science *360*, 656–660.

Segura, J., Ferretti, L., Ramos-Onsins, S., Capilla, L., Farré, M., Reis, F., Oliver-Bonet, M., Fernández-Bellón, H., Garcia, F., Garcia-Caldés, M., et al. (2013). Evolution of recombination in eutherian mammals: insights into mechanisms that affect recombination rates and crossover interference. Proc. Biol. Sci. *280*, 20131945.

Sharp, N.P., and Otto, S.P. (2016). Evolution of sex: Using experimental genomics to select among competing theories. BioEssays *38*, 751–757.

Stack, S.M., Royer, S.M., Shearer, L.A., Chang, S.B., Giovannoni, J.J., Westfall, D.H., White, R.A., and Anderson, L.K. (2009). Role of fluorescence in situ hybridization in sequencing the tomato genome. Cytogenet. Genome Res. *124*, 339–350.

Stapley, J., Feulner, P.G.D., Johnston, S.E., Santure, A.W., and Smadja, C.M. (2017). Recombination: the good, the bad and the variable. Philos. Trans. R Soc. Lond. B Biol. Sci. *372*, 20170279.

Storlazzi, A., Tessé, S., Gargano, S., James, F., Kleckner, N., and Zickler, D. (2003). Meiotic double-strand breaks at the interface of chromosome movement, chromosome remodeling, and reductional division. Genes Dev. *17*, 2675–2687.

Sun, F., Oliver-Bonet, M., Liehr, T., Starke, H., Turek, P., Ko, E., Rademaker, A., and Martin, R.H. (2006). Variation in MLH1 distribution in recombination maps for individual chromosomes from human males. Hum. Mol. Genet. *15*, 2376–2391.

Tease, C., and Hultén, M.A. (2004). Inter-sex variation in synaptonemal complex lengths largely determine the different recombination rates in male and female germ cells. Cytogenet. Genome Res. *107*, 208–215.

Tessé, S., Storlazzi, A., Kleckner, N., Gargano, S., and Zickler, D. (2003). Localization and roles of Ski8p protein in Sordaria meiosis and delineation of three mechanistically distinct steps of meiotic homolog juxtaposition. Proc. Natl. Acad. Sci. USA *100*, 12865–12870.

Veller, C., Kleckner, N., and Nowak, M.A. (2019). A rigorous measure of genome-wide genetic shuffling that takes into account crossover positions and Mendel's second law. Proc. Natl. Acad. Sci. USA *116*, 1659–1668.

Wang, J., Fan, H.C., Behr, B., and Quake, S.R. (2012). Genome-wide single-cell analysis of recombination activity and de novo mutation rates in human sperm. Cell *150*, 402–412.

Wang, S., Zickler, D., Kleckner, N., and Zhang, L. (2015). Meiotic crossover patterns: obligatory crossover, interference and homeostasis in a single process. Cell Cycle *14*, 305–314.

Wang, S., Hassold, T., Hunt, P., White, M.A., Zickler, D., Kleckner, N., and Zhang, L. (2017). Inefficient crossover maturation underlies elevated aneuploidy in human female meiosis. Cell *168*, 977–989.e17.

White, M.A., Wang, S., Zhang, L., and Kleckner, N. (2017). Quantitative modeling and automated analysis of meiotic recombination. Methods Mol. Biol. *1471*, 305–323.

Williams, G.C. (1975). Sex and Evolution (Princeton University).

Wiser, M.J., Ribeck, N., and Lenski, R.E. (2013). Long-term dynamics of adaptation in asexual populations. Science *342*, 1364–1367.

Zhang, L., Espagne, E., de Muyt, A., Zickler, D., and Kleckner, N.E. (2014a). Interference-mediated synaptonemal complex formation with embedded crossover designation. Proc. Natl. Acad. Sci. USA *111*, E5059–E5068.

Zhang, L., Liang, Z., Hutchinson, J., and Kleckner, N. (2014b). Crossover patterning by the beam-film model: analysis and implications. PLoS Genet. *10*, e1004042.

Zhang, L., Wang, S., Yin, S., Hong, S., Kim, K.P., and Kleckner, N. (2014c). Topoisomerase II mediates meiotic crossover interference. Nature *511*, 551–556.

Zhao, H., McPeek, M.S., and Speed, T.P. (1995). Statistical analysis of chromatid interference. Genetics *139*, 1057–1065.

Zickler, D., and Kleckner, N. (1999). Meiotic chromosomes: integrating structure and function. Annu. Rev. Genet. *33*, 603–754.

STAR★METHODS

KEY RESOURCES TABLE

REAGENT or RESOURCE	SOURCE	IDENTIFIER
Software and Algorithms		
Beam-Film Applications	Zhang et al., 2014b	https://app.box.com/s/hv91q2nrtq0cp9n8iy9m
MATLAB	MathWorks	N/A
GraphPad Prism	GraphPad Software, Inc.	N/A
Other		
Data used in this paper	See "Data Sources and Availability"	N/A

EXPERIMENTAL MODEL AND SUBJECT DETAILS

No cell culture was used in this work.

CONTACT FOR REAGENT AND RESOURCE SHARING

Further information and requests for resources and reagents should be directed to Nancy Kleckner at kleckner@fas.harvard.edu.

METHOD DETAILS

Data acquisition

Methodology for acquisition of analyzed data are given in primary references as follows: Human data are from refs. Gruhn et al., 2013; Sun et al., 2006; Oliver-Bonet et al., 2007; Lian et al., 2008; Lu et al., 2012; Hou et al., 2013 (provided by T. Hassold, F. Sun, M. Oliver-Bonet and S. Xie, respectively). Tomato data are from refs. Lhuissier et al., 2007 and Anderson et al., 2014; Sordaria data are from ref. De Muyt et al., 2014 and provided by D. Zickler; Tiger and elephant shrew data are from ref. Segura et al., 2013 and provided by A. Ruiz-Herrera. All data are aggregated for easy access in Table S1.

Co-variation analysis

(Figures 2, 4, 5, and S2) Co-variations of chromosome axis lengths or CO numbers were quantified by Pearson's linear correlation coefficient between individual chromosome pairs (Figures 2B, 4B, 5C, S2D, and S2E), between two chromosome groups (e.g., Figures 2A, 2D, 4A, 4D, and 5C) and also between one chromosome and all the rest of chromosomes in the nucleus (Figures S2B and S2C). For correlation analysis between two chromosome groups, each group is assigned the same numbers of chromosomes if the organism has an even number of chromosomes, or one group is assigned one more chromosome than the other if the organism has an odd number of chromosomes. The same method is also used to analyze the correlations between axis lengths and the numbers of recombination events (Figure S2G).

Coefficient of variation analysis

(Figures 1, 2, 3, 5, S1, and S2; Table 1) The observed distribution of CO numbers or axis lengths was plotted with the assistance of GraphPad Prism (GraphPad Software, Inc.) and quantified by the coefficient of variation (CV) which is the quotient of the standard deviation to the mean.

Variability index analysis

(Figures 1, 3, 5, S1, and S2) The total number of recombination events per nucleus observed experimentally varies much more broadly than predicted based on the hypothesis of independence across chromosomes within nuclei (Text and below), with more nuclei having higher recombination and also more nuclei having less recombination. Both distributions are well fit by a normal distribution. The percentages of nuclei with more recombination and with less recombination can be easily calculated by directly comparing the observed and the predicted distributions of COs per nucleus (or the corresponding best-fit normal distribution curves) (Figure 1C). We name this empirically useful parameter the "variability index" (VI; Figures 1D, 1G, 5B, S1F, and S2A). The variability index for axis length is calculated according to the same method (Figures 3B, 3C, 3F, and S1H).

Sorting bivalents randomly into single nuclei

(Figures 1, 3, 5, S1, and S2) For experimental data, for each chromosome, the bivalents from all analyzed nuclei were pooled. For simulated data, the population of simulated bivalents for each chromosome was similarly pooled. For each pseudo nucleus one bivalent was randomly picked from each of the pools corresponding to the different chromosomes in the organism in question (e.g., for human male, each of the 22 pools corresponding to the 22 autosomes). By doing this, each bivalent in a pseudo nucleus is completely independent of all of the other bivalents in that same nucleus with respect to both its CO number and axis length. Importantly, this random sorting does not alter the degree of variation, across nuclei, of CO number and axis length for a given chromosome (not shown).

Best-fit simulations for CO patterns

(Figures 5 and S3) Best-fit simulations used in this study were done by a program developed based on the beam-film model (a.k.a. the "fill-in-the-holes" model). Both the model and the program/simulations have already been described in detail (Zhang et al., 2014b, 2014c; White et al., 2017; Kleckner et al., 2004). The program written in MATLAB is available at https://app.box.com/s/hv91q2nrtq0cp9n8iy9m.

The beam-film model was originally proposed to explain the CO designation process. Briefly, in this model, given an array of CO precursors on each chromosome, under a certain level of CO designation driving force, the most sensitive CO precursor will be designated to be a CO, which will be developed into a real CO after a complicated biochemical process. An inhibition signal (interference) will automatically emanate from the designation site immediately when it is designated and will then spread out along the chromosome in both directions. The inhibition signal will decrease the probability that another CO precursor can be designated, thus decreasing CO occurrence in the region around the CO-designation site. If another CO designation (and thus CO) occurs it will most likely occur far away from prior CO (designation) sites. These effects automatically generate the classical phenomenon of interference. In this process, as long as the driving force for CO-designation is strong enough (which would be tuned evolutionarily), it can ensure each chromosome obtains at least one CO (the "obligatory" CO). When the number of precursors is increased or decreased, the number of CO designations (thus COs) changes, but less than proportionately. This is the phenomenon of CO homeostasis, the strength of which has been shown to depend on the strength of CO interference (Wang et al., 2015). This effect occurs essentially because the chance that a given precursor will be affected by a spreading interference signal from a nearby CO-designation will be lesser or greater at lower and higher precursor densities.

Three types of parameters must be specified for best-fit simulations (White et al., 2017; Zhang et al., 2014b).

(1) Precursor parameters. Undifferentiated pre-CO recombination interactions are known as "precursors." The array of precursors on each bivalent is specified by: (i) the average number of precursors per bivalent (N); (ii) the extent to which precursor numbers vary among different nuclei (B) and (iii) the extent to which precursors are either randomly spaced, or tend to be evenly spaced, on each bivalent, given by parameter (E). Overall, the values of these precursor parameters define the positions of each precursor on each bivalent in the sample population.

(2) CO patterning/designation parameters. For a given precursor, whether it can be designated to be a potential CO or not depends on the balance of the designation driving force at this precursor site at the moment of CO-designation and the sensitivity of that particular precursor to that driving force. The maximum possible CO designation driving force is given by (Smax). The distribution of intrinsic precursor sensitivities is defined by a parameter (A). Finally, the effective strength of the CO designation driving force at a particular position at a particular point in the overall CO designation process will be attenuated by the effects of any CO interference signal that has spread across that position from nearby positions, at that particular time. The CO interference signal nucleated at one CO-designation site will dissipate with distance away from that site (exponentially, by the model) and the distance over which that dissipation occurs is given by a parameter (L). In a given simulation, to enable sequential CO-designations, the CO designation driving force is progressively increased, up to the level specified by Smax. Precursor sites thus undergo CO-designation in relation to the combined effects of their intrinsic sensitivities and the strength of the CO designation driving force as modulated by interference according to the parameter (L). These parameters will define each CO designation site (and thus each CO), on each bivalent in the sample population (usually 5000 bivalents total).

(3) CO maturation efficiency (M). Normally a CO designation site will develop into a completed CO after a complicated biochemical process. However any defects that occur after CO designation and before completion of the process will decrease the probability of a designation site becoming a CO. The probability that a CO-designation will escape such a defect and become a completed CO is the maturation efficiency (M). M = 1 in most cases, but can be less than 1 in other cases (e.g., Wang et al., 2017).

The best-fit parameters were first obtained for each of 22 autosomes without axis length variation as described previously (Wang et al., 2017). (1) Axis length variation was mimicked by mixing two such subpopulations obtained at different axis lengths, one with 20% longer, and the other one with 20% shorter, than the average in the experimental population. Because the number of CO precursors scales with axis length (Zhang et al., 2014b, 2014c) (above), precursor numbers used in the two subpopulations were also adjusted according to axis lengths. Moreover, the interference distance L was also adjusted to keep the same interference distance (in microns) in the two subpopulations. Other parameters are the same for the two subpopulations, being the best-fit parameters for

the single population without axis length variation. After these adjustments, the total population obtained by combining the two sub-populations has the same axis length variation as observed in the experimental data. (2) The experimental data showed that the correlations between individual chromosome axis lengths is ~0.65. To mimic this, for each of the 22 simulated autosomes, ~35% of simulated chromosomes from each of the two subpopulations were randomly extracted, mixed and then randomized. This decreased the correlation level for the whole populations to ~0.65.

Predicting CO numbers in gametes

Studies have shown that there is no/little chromatid interference during meiotic recombination (e.g., Zhao et al., 1995; Mancera et al., 2008). If so, a CO formed between any two nonsister chromatids does not affect the usage of those chromatids by any other COs in the same nucleus. Thus, each CO on a bivalent will be randomly allocated to two nonsister chromatids (thus gametes). Thus, CO patterns on each chromosome in each gamete can be predicted.

Decomposing total variance of COs per nucleus

Let X be the random variable "number of COs in a prophase nucleus," and X_k be the random variable "number of crossovers on chromosome k in a prophase nucleus" (there are n chromosomes in the haploid set). Then we have the decomposition

$$\underbrace{Var(X)}_{A_p} = Var\left(\sum_{k=1}^{n} X_k\right) = \underbrace{\sum_{k=1}^{n} Var(X_k)}_{B_p} + \underbrace{\sum_{i\neq j} Cov(X_i, X_j)}_{C_p}. \tag{2}$$

A_p is the total variance of CO number in prophase nuclei (subscript p for "prophase"), B_p is the contribution to A_p from intrinsic variability of CO number on individual chromosomes, and C_p is the contribution to A_p from CO covariation across chromosomes.

Now let Y be the random variable "number of COs in a gamete." Assuming no chromatid interference, COs are binomially sampled from prophase nuclei into gametes. Therefore, conditional on X, Y is binomially distributed with parameters X and 1/2. In particular,

$$\mathbb{E}[Y \mid X] = X/2 \qquad \textit{and} \qquad Var(Y \mid X) = X/4.$$

To find the unconditional variance of Y, we use the law of total variance:

$$Var(Y) = Var_X(\mathbb{E}[Y \mid X]) + \mathbb{E}_X[Var(Y \mid X)] = Var_X(X/2) + \mathbb{E}_X[X/4] = \frac{Var(X)}{4} + \frac{\mathbb{E}[X]}{4}. \tag{3}$$

The first term is the contribution to the variance of gamete CO number that is due to variance in prophase CO number, and the second term is the extra noise from random (binomial) sorting of prophase COs into gametes.

We want to decompose Var(Y) analogously to how we decomposed Var(X)—into a component due to "intrinsic" noise and a component due to CO covariation. Clearly, CO covariation in gametes can only systematically derive from CO covariation in prophase nuclei (again, assuming no chromatid interference), and so the appropriate partition of Var(Y) is:

$$A_g = Var(Y) = \frac{Var(X)}{4} + \frac{\mathbb{E}[X]}{4} = \frac{A_p + \overline{X}}{4} = \frac{B_p + C_p + \overline{X}}{4} = \underbrace{\frac{B_p + \overline{X}}{4}}_{B_g} + \underbrace{\frac{C_p}{4}}_{C_g}, \tag{4}$$

where $\overline{X}$ is shorthand for $\mathbb{E}[X]$, A_g is the total variance of CO number in gametes (subscript g for "gametes"), C_g is the contribution to A_g from CO covariation in prophase nuclei, and B_g is the contribution from variation in individual chromosomes' CO numbers and from the noise introduced in the random sampling of COs from prophase nuclei into gametes. It is easily shown that B_g and C_g can be written in a form similar to the terms in Equation (2).

Note the simple relationship between the contribution of CO covariation to total variance in prophase nuclei and gametes: $C_g = C_p/4$. This relationship is clearly observed when comparing the cytological data for prophase nuclei in male and female human with single-gamete sequencing data (Table 1).

From Eqs. (3) and (4), we can compare the contribution of CO covariation to total variance of CO number in prophase and gametes; i.e., we can compare C_p/A_p with C_g/A_g:

$$\frac{C_p/A_p}{C_g/A_g} = \frac{C_p/A_p}{\frac{C_p}{4}\Big/\frac{B_p + \overline{X} + C_p}{4}} = \frac{C_p/A_p}{C_p/(B_p + C_p + \overline{X})} = \frac{C_p/A_p}{C_p/(A_p + \overline{X})} = \frac{A_p + \overline{X}}{A_p} = 1 + \frac{\overline{X}}{A_p}.$$

From this, we observe:

- C/A is always reduced in gametes: $C_p/A_p > C_g/A_g$ because $1 + \overline{X}/A_p > 1$.
- The reduction is entirely captured by the size of the term $\overline{X}/A_p$, i.e., $\mathbb{E}[X]/Var(X)$.

In the term $\mathbb{E}[X]/Var(X)$, $\mathbb{E}[X]$ is proportional to the noise contributed to A_g by binomial sampling (which dilutes the effect of prophase CO covariation). $Var(X)$ is proportional to the contribution to A_g from CO variance in prophase nuclei (which preserves the effect of prophase CO covariation). If the former is large relative to the latter, then the reduction in *C/A* as we move to gametes is severe.

We can rewrite $\mathbb{E}[X]/Var(X) = 1/(\mathbb{E}[X]c_v^2(X))$, where $c_v^2(X)$ is the square of the coefficient of variation of X. From this, we can identify two reasons that the reduction in *C/A* from prophase nuclei to gametes in human female is not as severe as in human male. First, $\mathbb{E}[X]$ is larger in human females—there are more prophase COs, on average, in females than in males. The result of this is that the noise associated with binomial sampling of COs from nuclei into gametes is proportionately smaller in female than in male, because the sample size is bigger. Second, $c_v(X)$ is larger in female than in male—prophase CO number is disproportionately more variable in female than in male. In fact, among the two contributors to to the male-female difference in reduction of *C/A* moving from prophase to gametes, the contribution of "more female variance" (the ratio of $1/c_v^2(X)$ in male versus female) is larger than the contribution of "more COs in females" (the ratio of $1/\mathbb{E}[X]$ in male versus female) by a factor of about 2.3.

Population Genetic Modeling

General model

To model the effects of CO covariation across chromosomes requires multiple chromosomes (across which CO covariation can occur) and multiple loci per chromosome (between which COs can occur). The minimal model therefore involves two chromosomes, with two loci on each chromosome. The two loci on chromosome 1 are $\mathcal{A}$ and $\mathcal{B}$; the two loci on chromosome 2 are $\mathcal{C}$ and $\mathcal{D}$. Each locus segregates for two alleles: *A*/*a*, *B*/*b*, *C*/*c*, *D*/*d*. For simplicity, the model organism is taken to be a haploid with only one sex. The life-cycle is that haploid individuals undergo selection, then unite at random to form transient diploids, which undergo meiosis and segregate back into haploid gametes which are the offspring. Fitness is assigned to haplotypes (e.g., *AbcD*) rather than diploid genotypes. The relative fitness of haplotype *AbcD* in generation t is labeled $f_{AbcD}(t)$. We assume that the population is sufficiently large that random drift can be ignored.

Given some scheme of how selection acts in each generation and how this changes across generations, we shall be interested in the growth rates over time of populations employing different "covariation" strategies (i.e., the long-term geometric mean fitness of each population). In each sexual event in a given population, the probability that the alleles at loci $\mathcal{A}$ and $\mathcal{B}$ are shuffled in a gamete is r, and the probability that the alleles at $\mathcal{C}$ and $\mathcal{D}$ are shuffled in a gamete is also r. Segregation of loci on separate chromosomes follows Mendel's second law. r is held constant for every population we shall consider. Populations differ according to the degree of covariance of recombination events between the two locus pairs, as defined by the parameter κ. Let $R_{1,1}$ be the probability that the alleles at the locus pairs on both chromosomes are shuffled in a gamete, $R_{1,0}$ that the alleles at chromosome 1's pair are shuffled, but not chromosome 2's, $R_{0,1}$ that the alleles at chromosome 2's pair are shuffled, but not chromosome 1's, and $R_{0,0}$ that the alleles at neither locus pair are shuffled. Then

$$R_{1,1} = r^2 + \kappa, \quad R_{1,0} = r(1-r) - \kappa, \quad R_{0,1} = r(1-r) - \kappa, \quad R_{0,0} = (1-r)^2 + \kappa.$$

Under this model, κ is precisely the covariance of recombination events between the two locus pairs (as measured in gametes). Since the above probabilities must be between zero and one (inclusive), a restriction on κ is $\kappa \leq r(1-r)$. From this restriction, we define the scaled parameter $K = \kappa/[r(1-r)]$, so that $K = 0$ corresponds to no covariation and $K = 1$ corresponds to maximal covariation, with $K \in (0, 1)$ defining intermediate values of positive CO covariation.

In all of the fitness schemes we shall consider, there will be a "best" and/or "worst" set of alleles at any one time. Recombination is relevant because the best/worst genotypes change over time.

Recursion equations

Label the genotypes in the following order:

1	2	3	4	5	6	7	8	9	10	11	12	13	14	15	16
abcd	*Abcd*	*aBcd*	*abCd*	*abcD*	*ABcd*	*AbCd*	*AbcD*	*aBCd*	*aBcD*	*abCD*	*ABCd*	*ABcD*	*AbCD*	*aBCD*	*ABCD*

Let x_i^t be the frequency of genotype i in the current (t-th) generation, and suppose that selection this generation is such that the expected number of offspring of an individual with the i-th genotype is $2f_i^t$. Then the mean fitness of the population this generation is $F_t = \sum_{i=1}^{16} x_i^t f_i^t$. The geometric mean fitness from generation 1 to G is then

$$GMF = \left(\prod_{t=1}^{G} F_t\right)^{1/G} = exp\left(\frac{1}{G}\sum_{t=1}^{G} log(F_t)\right),$$

where the second formula is given because it is easier to compute for large G.

Let $y_i^t = x_i^t f_i^t / \sum_{j=1}^{16} x_j^t f_j^t$, and write

$$p_{ab}^t = y_1^t + y_4^t + y_5^t + y_{11}^t; \quad p_{AB}^t = y_6^t + y_{12}^t + y_{13}^t + y_{16}^t;$$

$$p_{Ab}^t = y_2^t + y_7^t + y_8^t + y_{14}^t; \quad p_{aB}^t = y_3^t + y_9^t + y_{10}^t + y_{15}^t;$$

$$p_{cd}^t = y_1^t + y_2^t + y_3^t + y_6^t; \quad p_{CD}^t = y_{11}^t + y_{14}^t + y_{15}^t + y_{16}^t;$$

$$p_{Cd}^t = y_4^t + y_7^t + y_9^t + y_{12}^t; \quad p_{cD}^t = y_5^t + y_8^t + y_{10}^t + y_{13}^t;$$

and

$$D_{\mathcal{AB}|cd}^t = y_6^t p_{ab}^t + y_1^t p_{AB}^t - y_2^t p_{aB}^t - y_3^t p_{Ab}^t; \quad D_{\mathcal{AB}|Cd}^t = y_{12}^t p_{ab}^t + y_4^t p_{AB}^t - y_7^t p_{aB}^t - y_9^t p_{Ab}^t;$$

$$D_{\mathcal{AB}|cD}^t = y_{13}^t p_{ab}^t + y_5^t p_{AB}^t - y_8^t p_{aB}^t - y_{10}^t p_{Ab}^t; \quad D_{\mathcal{AB}|CD}^t = y_{16}^t p_{ab}^t + y_{11}^t p_{AB}^t - y_{14}^t p_{aB}^t - y_{15}^t p_{Ab}^t;$$

$$D_{\mathcal{CD}|ab}^t = y_{11}^t p_{cd}^t + y_1^t p_{CD}^t - y_4^t p_{cD}^t - y_5^t p_{Cd}^t; \quad D_{\mathcal{CD}|Ab}^t = y_{14}^t p_{cd}^t + y_2^t p_{CD}^t - y_7^t p_{cD}^t - y_8^t p_{Cd}^t;$$

$$D_{\mathcal{CD}|aB}^t = y_{15}^t p_{cd}^t + y_3^t p_{CD}^t - y_9^t p_{cD}^t - y_{10}^t p_{Cd}^t; \quad D_{\mathcal{CD}|AB}^t = y_{16}^t p_{cd}^t + y_6^t p_{CD}^t - y_{12}^t p_{cD}^t - y_{13}^t p_{Cd}^t;$$

and $D_{\mathcal{ABCD}}^t = y_1^t y_{16}^t + y_6^t y_{11}^t + y_7^t y_{10}^t + y_8^t y_9^t - y_2^t y_{15}^t - y_3^t y_{14}^t - y_4^t y_{13}^t - y_5^t y_{12}^t$.

Then, in the next generation,

$$x_1^{t+1} = \frac{1}{2}\left(y_1^t + p_{ab}^t p_{cd}^t - rD_{\mathcal{AB}|cd}^t - rD_{\mathcal{CD}|ab}^t + (r^2+\kappa)D_{\mathcal{ABCD}}^t\right),$$

$$x_2^{t+1} = \frac{1}{2}\left(y_2^t + p_{Ab}^t p_{cd}^t + rD_{\mathcal{AB}|cd}^t - rD_{\mathcal{CD}|Ab}^t - (r^2+\kappa)D_{\mathcal{ABCD}}^t\right),$$

$$x_3^{t+1} = \frac{1}{2}\left(y_3^t + p_{aB}^t p_{cd}^t + rD_{\mathcal{AB}|cd}^t - rD_{\mathcal{CD}|aB}^t - (r^2+\kappa)D_{\mathcal{ABCD}}^t\right),$$

$$x_4^{t+1} = \frac{1}{2}\left(y_4^t + p_{ab}^t p_{Cd}^t - rD_{\mathcal{AB}|Cd}^t + rD_{\mathcal{AB}|ab}^t - (r^2+\kappa)D_{\mathcal{ABCD}}^t\right),$$

$$x_5^{t+1} = \frac{1}{2}\left(y_5^t + p_{ab}^t p_{cD}^t - rD_{\mathcal{AB}|cD}^t + rD_{\mathcal{CD}|ab}^t - (r^2+\kappa)D_{\mathcal{ABCD}}^t\right),$$

$$x_6^{t+1} = \frac{1}{2}\left(y_6^t + p_{AB}^t p_{cd}^t - rD_{\mathcal{AB}|cd}^t - rD_{\mathcal{CD}|AB}^t + (r^2+\kappa)D_{\mathcal{ABCD}}^t\right),$$

$$x_7^{t+1} = \frac{1}{2}\left(y_7^t + p_{Ab}^t p_{Cd}^t + rD_{\mathcal{AB}|Cd}^t + rD_{\mathcal{CD}|Ab}^t + (r^2+\kappa)D_{\mathcal{ABCD}}^t\right),$$

$$x_8^{t+1} = \frac{1}{2}\left(y_8^t + p_{Ab}^t p_{cD}^t + rD_{\mathcal{AB}|cD}^t + rD_{\mathcal{CD}|Ab}^t + (r^2+\kappa)D_{\mathcal{ABCD}}^t\right),$$

$$x_9^{t+1} = \frac{1}{2}\left(y_9^t + p_{aB}^t p_{Cd}^t + rD_{\mathcal{AB}|Cd}^t + rD_{\mathcal{CD}|aB}^t + (r^2+\kappa)D_{\mathcal{ABCD}}^t\right),$$

$$x_{10}^{t+1} = \frac{1}{2}\left(y_{10}^t + p_{aB}^t p_{cD}^t + rD_{\mathcal{AB}|cD}^t + rD_{\mathcal{CD}|aB}^t + (r^2+\kappa)D_{\mathcal{ABCD}}^t\right),$$

$$x_{11}^{t+1} = \frac{1}{2}\left(y_{11}^t + p_{ab}^t p_{CD}^t - rD_{\mathcal{AB}|CD}^t - rD_{\mathcal{CD}|ab}^t + (r^2+\kappa)D_{\mathcal{ABCD}}^t\right),$$

$$x_{12}^{t+1} = \frac{1}{2}\left(y_{12}^t + p_{AB}^t p_{Cd}^t - rD_{\mathcal{AB}|Cd}^t + rD_{\mathcal{CD}|AB}^t - (r^2+\kappa)D_{\mathcal{ABCD}}^t\right),$$

$$x_{13}^{t+1} = \frac{1}{2}\left(y_{13}^{t} + p_{AB}^{t}p_{cD}^{t} - rD_{\mathcal{AB}|cD}^{t} + rD_{\mathcal{CD}|AB}^{t} - \left(r^2+\kappa\right)D_{\mathcal{ABCD}}^{t}\right),$$

$$x_{14}^{t+1} = \frac{1}{2}\left(y_{14}^{t} + p_{Ab}^{t}p_{CD}^{t} + rD_{\mathcal{AB}|CD}^{t} - rD_{\mathcal{CD}|Ab}^{t} - \left(r^2+\kappa\right)D_{\mathcal{ABCD}}^{t}\right),$$

$$x_{15}^{t+1} = \frac{1}{2}\left(y_{15}^{t} + p_{aB}^{t}p_{CD}^{t} + rD_{\mathcal{AB}|CD}^{t} - rD_{\mathcal{CD}|aB}^{t} - \left(r^2+\kappa\right)D_{\mathcal{ABCD}}^{t}\right),$$

$$x_{16}^{t+1} = \frac{1}{2}\left(y_{16}^{t} + p_{AB}^{t}p_{CD}^{t} - rD_{\mathcal{AB}|CD}^{t} - rD_{\mathcal{CD}|AB}^{t} + \left(r^2+\kappa\right)D_{\mathcal{ABCD}}^{t}\right).$$

Given these recursion equations, a set of starting frequencies, and the timing and nature of changes in the selective environment, the dynamics are fully specified.

Nature of selection

Selection acts symmetrically on combinations of alleles at the two locus pairs, so that, for example, at a given time, haplotypes *AB* and *ab* are fittest at the first locus pair and haplotypes *Cd* and *cD* are fittest at the second locus pair. This ensures that every allele's frequency is always 1/2, i.e., that symmetric polymorphism is maintained at each locus in the long run. Fitness is then given by a function $\phi(i,j)$, where $i = 1$ (resp. $i = -1$) if a genotype has one of the "right" (resp. "wrong") combinations at the first locus pair, and the same for j at the second locus pair. The strength of selection is given by the parameter s. We consider three selection scenarios:

I. Selection acts so that only the very fittest genotypes have a selective advantage:

$\phi(i,j) = 1+s$ if $i = j = 1$, but $\phi(i,j) = 1$ otherwise.

II. Selection acts more evenly across genotypes (multiplicatively across chromosomes):

$\phi(i,j) = (1 + i\tilde{s})(1 + j\tilde{s})$, with $(1+\tilde{s})^2 = 1 + s$.

III. Selection acts so that only the very least fit genotypes are at a selective disadvantage:

$\phi(i,j) = 1/(1+s)$ if $i = j = -1$, but $\phi(i,j) = 1$ otherwise.

In each case, the relative fitness difference between the fittest and least fit genotype is 1+*s*.

Timing and nature of change in selective environment

Each generation, there is a probability $1/T$ that the environment changes, constant and independent across generations. Therefore, the average time between environmental changes is T generations, though there is some variance in these inter-change "stasis" periods. When the environment changes, a new set of favored alleles is chosen. We consider two models for this:

1. When a selective change occurs, with probability (1-*p*)/2 it is only at the first locus pair (e.g., changing the favored combinations from *AB* and *ab* to *Ab* and *aB*), with probability (1-*p*)/2 it is only at the second locus pair, and with probability *p* it is at both locus pairs.
2. When a selective change occurs, a completely new set of favored combinations is chosen, with each (except the current best combination) equally likely.

Simulation setup

In each simulation run, we fix the selective regime (I, I, or III), the nature of selective changes (1 or 2), and the various parameters (including *K*, the degree of CO covariation). We start the population with equal frequencies of each genotype (i.e., frequency 1/16 for each of the 16 genotypes), with genotypes *ABCD*, *ABcd*, *abCD*, and *abcd* being the fittest. For a "burn-in" period of 10^5 generations and a main period of 10^7 generations, we choose the generations in which selective change occurs, and the nature of each selective change (favored combination changes on chromosome 1 only, or chromosome 2 only, or both chromosomes). We then iterate the recursion equations above for the 10^5 burn-in generations (during which the selective environment will change, on average, $10^5/T$ times), not tracking population fitness. The genotype frequencies at the end of the burn-in period are then used as the starting frequencies for the main phase. Across the 10^7 subsequent generations, in each generation t we keep track of population fitness F_t. At the end of the 10^7 generations, we calculate the geometric mean fitness of the population, as described above.

Caveats, and possible extensions

The model we employed is, by necessity, highly simplified, ignoring a number of biological complexities that could plausibly affect the degree to which CO covariation is advantageous. For example, (i) while genomes contain many loci under selection, and thus subject to CO covariation effects, our model contains only four loci. Extending the model to contain many loci would be valuable. Analytical tractability might be preserved by assuming that selective effects at these loci are weak relative to the force

of recombination (Barton 1995), which would also allow for the continual introduction of deleterious mutations at the various loci, as occurs in the genomes of natural populations. (ii) We have also assumed that the time until the next environmental change is geometrically distributed. It would be interesting to study a wider range of environmental fluctuation regimes. (iii) Our inclusion of only two chromosomes elevates the importance of COs as a source of genetic shuffling, relative to independent assortment of homologous chromosomes. With more chromosomes, independent assortment becomes the greater contributor (Veller et al., 2019)—it would be interesting to study if this has a quantitative effect on the selective advantage of CO covariation.

QUANTIFICATION AND STATISTICAL ANALYSIS

Details of Statistical Analyses

Co-variation analysis

(Figures 2A, 2B, 2D, 4A, 4B, 4D, 5C, S2B–S2E, and S2G) Pearson's linear correlation coefficient is used for co-variation analysis.

Coefficient of variation analysis

(Figures 1B, 1E, 1F, 2E, 3A, 3D, 3E, 5A, S1E, and S1G; Table 1) The variation levels of CO numbers or axis lengths were plotted with the assistant of GraphPad Prism (GraphPad Software, Inc.) and quantified by the coefficient of variation (CV) which is the quotient of the standard deviation to the mean. The 95% confidence intervals (CI) for the CV were estimated by bootstrap resampling using MATLAB (The MathWorks, Inc) and the standard error (SE) was estimated from the 95% CI according to $SE = \Delta CI/3.92$

Standard Errors

Figures 1D, 1G, 2A, right, 2B, 3C, 3F, 4A, right, 4B, 5B, 5C, S1E–S1H, S2B, right, S2C, right, S2E, and S2F.

Standard deviations

Figures 1B, 1E, 1F, 3A, 3D, 3E, and 5A.

DATA AND SOFTWARE AVAILABILITY

Software availability

Best-fit simulations used in this study were done by a program developed based on the beam-film model (a.k.a. "fill-in-the-holes" model). Both the model and the program/simulations have already been described in detail (Zhang et al., 2014b, 2014c; White et al., 2017; Kleckner et al., 2004). The program written in MATLAB is available at https://app.box.com/s/hv91q2nrtq0cp9n8iy9m.

Cell

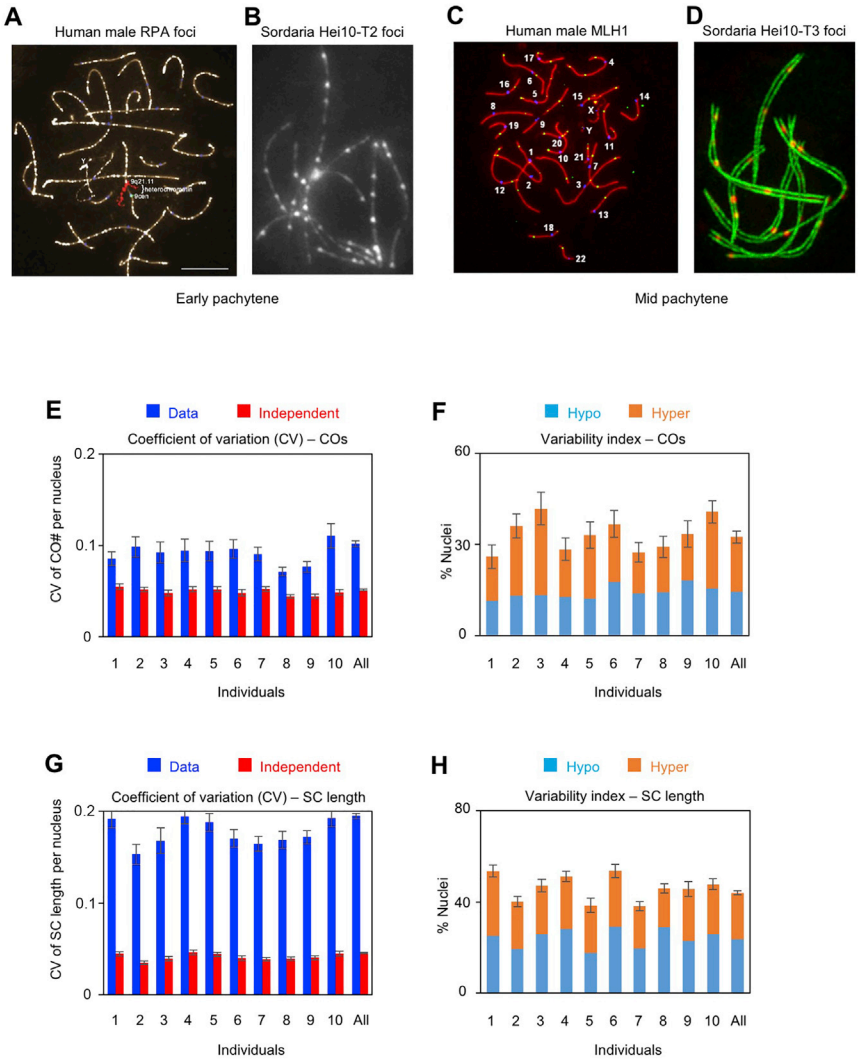

Figure S1. Cytological Visualization of Early Recombination Interactions and Crossovers, and Hyper-variability of COs and Axis Lengths among Nuclei from the Same Individual, Related to Figures 1, 2, 3, and 4

(A and B) During meiosis, DSB-mediated early recombination intermediates can be seen cytologically on synaptonemal complexes (SCs) during early pachytene, e.g., RPA foci in human male (A) and Hei10 T2 foci in Sordaria (B). (C and D) Among the large number of early recombination interactions, a small subset eventually mature into COs. Recombination complexes corresponding to COs can be visualized along SCs by immunostaining with CO-specific proteins, illustrated here for MLH1 foci in human male and Hei10 T3 foci in Sordaria. The rest of the early recombination interactions are matured into noncrossovers (NCOs). The picture of panel A is from Oliver-Bonet et al., 2007; Pictures of panels B and D are provided by D. Zickler; the picture of panel C is provided by F. Sun. (E-H): Comparable hyper-variability of COs (E and F) and axis lengths (G and H) is seen among nuclei from each of 10 human males examined. Thus the hyper-variability is an intrinsic property of the meiotic program that is not attributable to individual-to-individual variation. x axis: 1-10 represents each of the 10 individuals, and "All" represents the total of the 10 individuals. Sample sizes, n = 78, 89, 51, 79, 76, 48, 96, 104, 75, 59 for the 10 individuals, respectively. Error bars = SE.

A Normal Distribution Analysis of Experimental Data

	Best-fit Parameters for Normal distribution			Normal distribution			Data
	Mean	Standard deviation		Fraction of nuclei		Variability Index	Variability Index
		Data	Independence	Hypo-CO	Hyper-CO		
Human male	49.33	5.03	2.54	0.16	0.16	0.32	0.33
Human female	83.04	4.84	16.24	0.26	0.26	0.52	0.51
Sordaria	22.14	2.98	1.91	0.11	0.11	0.21	0.22
Tomato	17.11	3.37	1.94	0.13	0.13	0.26	0.21
Tiger	63.37	6.86	3.40	0.16	0.16	0.33	0.45
E. Shrew	27.57	3.64	1.63	0.18	0.18	0.36	0.33

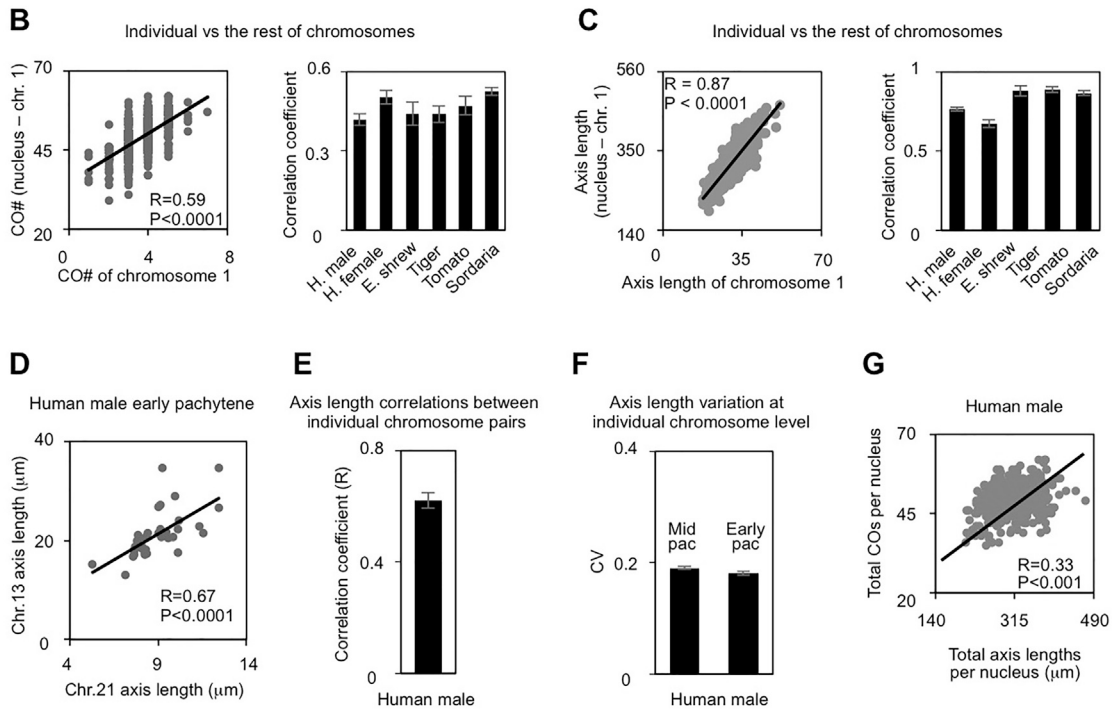

Figure S2. Normal Distribution of CO per-Nucleus Frequencies and Origin of per-Nucleus Covariation of Recombination Event Numbers in per-Nucleus Covariation of Bivalent Axis Lengths, Related to Figures 1, 2, 3, and 4

(A) The distributions of the number of COs per nucleus from both the experimental data and the *in silico* nuclei reconstructed based on the hypothesis of independence are well fit by normal distribution. The fractions of "hyper-CO" and "hypo-CO" nuclei and the corresponding variability index are calculated by directly comparing the observed and the predicted distributions of COs per nucleus (or the corresponding best-fit normal distribution curves; text). (B) The number of COs on each bivalent is positively correlated with the total number of COs on the rest of the bivalents in that nucleus. (C) The axis length of each bivalent is correlated with the total axis length for the rest of the bivalents in that nucleus. Sample sizes, same as for corresponding CO data in Figures 1B–1G. (D and E) The axis lengths of different individual chromosomes are also correlated at early pachytene as shown for one chromosome pair in (D) and for all pairs in (E). (F) Comparable levels of axis length variation are seen for individual chromosomes between early and mid pachytene (average for all chromosomes). (G) The number of COs directly positively correlates with axis length on a per-nucleus basis for COs. Error bars = SE.

A

The best-fit simulation parameters used in this study

	Longer axis		shorter axis	
Chromosome	N	L	N	L
1	23	0.168	15	0.25
2	20	0.184	13	0.28
3	16	0.208	11	0.31
4	14	0.24	9	0.36
5	14	0.24	10	0.36
6	14	0.256	9	0.38
7	14	0.256	9	0.38
8	11	0.312	7	0.47
9	12	0.296	8	0.44
10	11	0.28	7	0.42
11	11	0.28	8	0.42
12	11	0.28	8	0.42
13	8	0.336	5	0.50
14	8	0.336	5	0.50
15	9	0.336	6	0.50
16	8	0.328	6	0.49
17	9	0.328	6	0.49
18	6	0.352	4	0.53
19	8	0.336	5	0.50
20	5	0.336	4	0.50
21	3	0.72	2	1.08
22	4	0.56	3	0.84

B

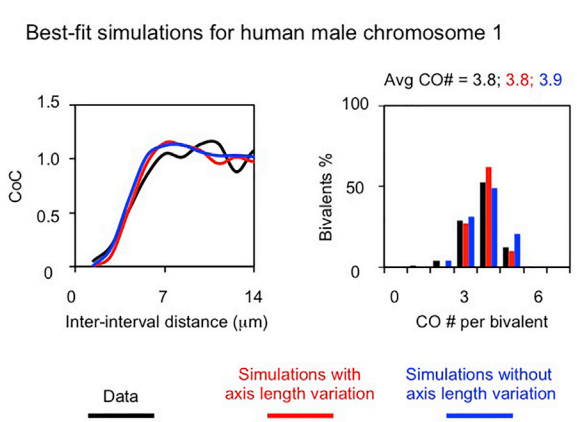

Figure S3. The Best-Fit Simulations, Related to Figures 1, 2, 3, 4, and 5

(A) The best-fit simulation parameters with axis length variations used in this study (STAR Methods). (B) The simulations with and without axis length variations can fit experimental CO patterns very well for Coefficient of Coincidence (CoC) relationships, which describe the effects of CO interference (left), and for the average number and distribution of COs per bivalent (right), as illustrated for human male chromosome 1.

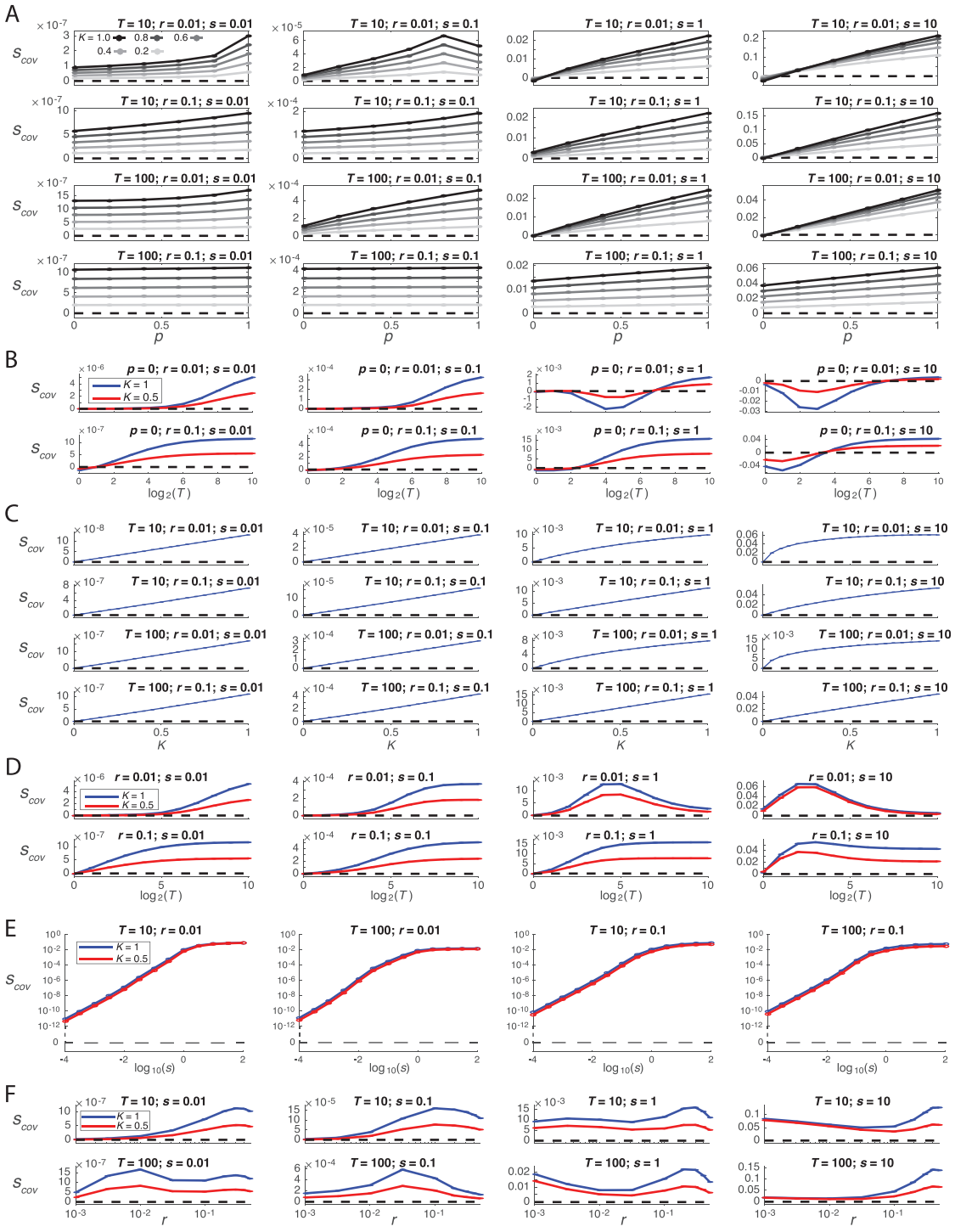

Figure S4. CO Covariation Is Favored under a Wide Range of Conditions When Selection Acts So that Only the Very Fittest Have a Reproductive Advantage (selection scenario I, STAR Methods), Related to Figure 6

(A) The selective advantage of CO covariation, s_{cov}, plotted across values of p, the probability that a given environmental change selects for new genetic combinations at both locus pairs, instead of just one locus pair. CO covariation is favored ($s_{cov} > 0$) under almost all parameter configurations. (B) Fixing $p = 0$, so that environmental changes are always associated with a selective change at only one locus pair (disfavoring CO covariation), CO covariation is nonetheless usually beneficial, and its advantage tends to increase with T, the average period between environmental changes. (C-F) Effects of various parameters on the

(legend continued on next page)

advantage of CO covariation, in the simpler model where, if the environment changes, a random new best combination of alleles is chosen, with each alternative equally likely. (C) The selective advantage of CO covariation, s_{cov}, changes monotonically with the degree of CO covariation, K. (D) s_{cov} generally increases with T, except when the recombination rate between each locus pair is small (r small) and selection is strong (s large). (E) s_{cov} changes monotonically with the strength of selection, s. (F) The dependence of s_{cov} on the rate of recombination between each locus pair, r, is non-monotonic.

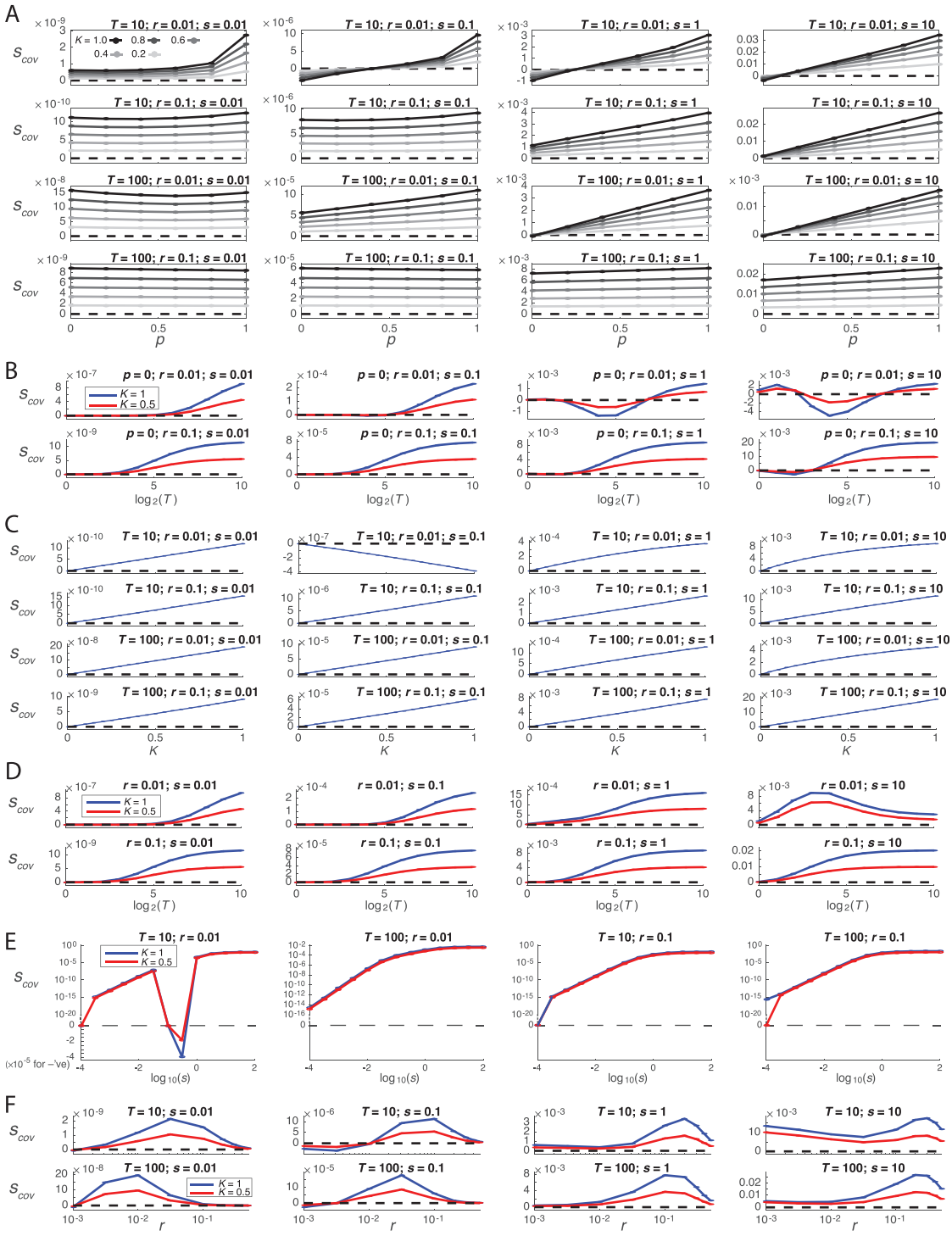

Figure S5. CO Covariation Is Still Favored under a Wide Range of Conditions When Selection Acts in an Even Fashion across Genotypes (selection scenario II, STAR Methods), Related to Figure 6

(A) The selective advantage of CO covariation, s_{cov}, plotted across values of p, the probability that a given environmental change selects for new genetic combinations at both locus pairs, instead of just one locus pair. CO covariation is favored ($s_{cov} > 0$) under almost all parameter configurations. (B) Fixing $p = 0$, so that environmental changes are always associated with a selective change at only one locus pair (disfavoring CO covariation), CO covariation is nonetheless usually beneficial, and its advantage tends to increase with T, the average period between environmental changes. (C-F) Effects of various parameters on the

(legend continued on next page)

advantage of CO covariation, in the simpler model where, if the environment changes, a random new best combination of alleles is chosen, with each alternative equally likely. (C) The selective advantage of CO covariation, s_{cov}, changes monotonically with the degree of CO covariation, K. (D) s_{cov} generally increases with T, except when the recombination rate between each locus pair is small (r small) and selection is strong (s large). (E) s_{cov} generally changes monotonically with the strength of selection, s. (F) The dependence of s_{cov} on the rate of recombination between each locus pair, r, is again non-monotonic.

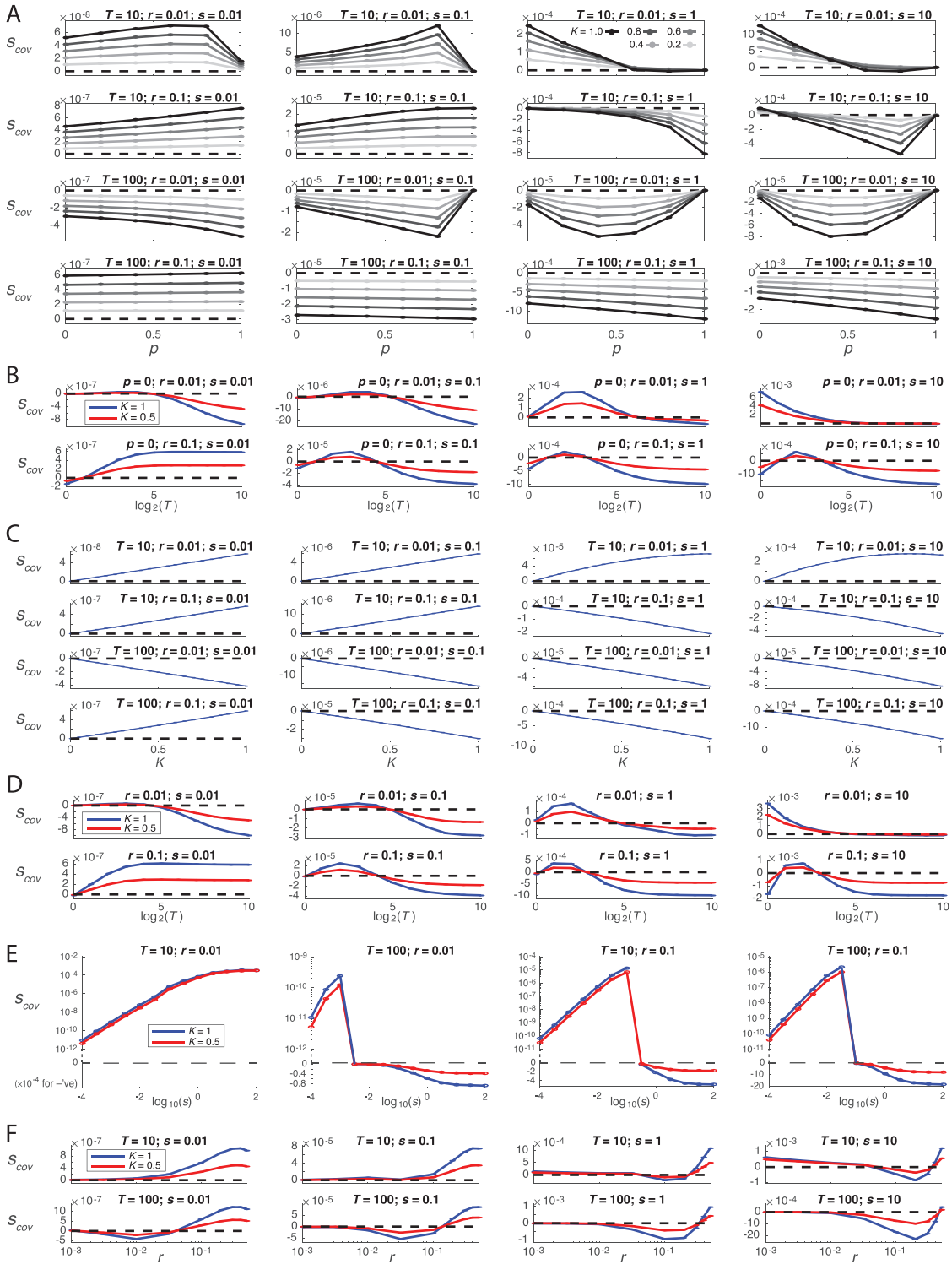

Figure S6. CO Covariation Is Favored Less Often when Selection Acts Such that Only the Least Fit Genotype Is at an Appreciable Selective Disadvantage (selection scenario III, STAR Methods), Related to Figure 6

(A) The selective advantage of CO covariation, s_{cov}, plotted across values of p, the probability that a given environmental change selects for new genetic combinations at both locus pairs, instead of just one locus pair. CO covariation is favored ($s_{cov} > 0$) when the average period between environmental changes, T, is small, but not when T is large. The magnitude of the selective advantage/disadvantage of covariation under scenario III is typically much smaller than under selection scenarios I and II. (B) Fixing $p = 0$, so that environmental changes are always associated with a selective change at only one locus pair (disfavoring CO

(legend continued on next page)

covariation), CO covariation's selective effect is non-monotonic in T, but tends to decline with T at larger values. (C-F) Effects of various parameters on the advantage of CO covariation, in the simpler model where, if the environment changes, a random new best combination of alleles is chosen, with each alternative equally likely. (C) The selective advantage of CO covariation, s_{cov}, changes monotonically with the degree of CO covariation, K. (D) s_{cov} shows non-monotonic dependence on T, though tends to decline as T increases at higher values. (E) s_{cov} generally changes monotonically with the strength of selection, s, for positive and negative values of s_{cov}. (F) The dependence of s_{cov} on the rate of recombination between each locus pair, r, is again non-monotonic.